Key Points:
- A framework is proposed to identify the magnitude and direction of longshore sediment transport from patterns of atmospheric variability
- One-line shoreline change simulations reveal previously unquantified timescales of coastal change
- Interannual and multidecadal wave climate variability dominates long-term evolution of headland-bound littoral cells in Oregon

A Climate Index Optimized for Longshore Sediment Transport Reveals Interannual and Multidecadal Littoral Cell Rotations

Dylan Anderson[1] (iD), **Peter Ruggiero**[2] (iD), **José A. A. Antolínez**[3], **Fernando J. Méndez**[3] (iD), **and Jonathan Allan**[4]

[1]College of Engineering, Oregon State University, Corvallis, OR, USA, [2]College of Earth, Ocean, and Atmospheric Sciences, Oregon State University, Corvallis, OR, USA, [3]Department of Sciences and Techniques in Water and Environment, University of Cantabria, Santander, Spain, [4]Oregon Department of Geology and Mineral Industries, Newport, OR, USA

Abstract A recent 35-year endpoint shoreline change analysis revealed significant counterclockwise rotations occurring in north-central Oregon, USA, littoral cells that extend 10s of kilometers in length. While the potential for severe El Niños to contribute to littoral cell rotations at seasonal to interannual scale was previously recognized, the dynamics resulting in persistent (multidecadal) rotation were unknown, largely due to a lack of historical wave conditions extending back multiple decades and the difficulty of separating the timescales of shoreline variability in a high energy region. This study addresses this question by (1) developing a statistical downscaling framework to characterize wave conditions relevant for longshore sediment transport during data-poor decades and (2) applying a one-line shoreline change model to quantitatively assess the potential for such large embayed beaches to rotate. A climate INdex was optimized to capture variability in longshore wave power as a proxy for potential LOngshore Sediment Transport (LOST_IN), and a procedure was developed to simulate many realizations of potential wave conditions from the index. Waves were transformed dynamically with Simulating Waves Nearshore to the nearshore as inputs to a one-line model that revealed shoreline rotations of embayed beaches at multiple time and spatial scales not previously discernible from infrequent observations. Model results indicate that littoral cells respond to both interannual and multidecadal oscillations, producing comparable shoreline excursions to extreme El Niño winters. The technique quantitatively relates morphodynamic forcing to specific climate patterns and has the potential to better identify and quantify coastal variability on timescales relevant to a changing climate.

Plain Language Summary The global climate forces large atmospheric weather patterns which in turn create the ocean waves ultimately responsible for erosion at the coastline. As the global climate changes, so too can long-term trends in coastal erosion. We have developed a technique to directly relate weather patterns to coastal change resulting from the transport of sediment along beaches and applied the method to investigate shoreline change trends in Oregon, USA, from the 1950s to the present. Counter to previous understanding, climate change on the timescale of multiple decades is responsible for which municipalities in Oregon experience persistent erosion hazards. The technique revealed the importance of large-scale climate in changing storm tracks approaching Oregon across the North Pacific. The technique developed for identifying climate patterns relevant to local coastal dynamics could be a useful predictive tool for understanding how the coast may evolve on timescales relevant for coastal managers into the 21st century.

1. Introduction

Beaches around the world are currently experiencing chronic erosion, which is only expected to worsen due to global climate change (e.g., Vitousek, Barnard, Limber, 2017). The nearshore science community has recognized that predicting coastal vulnerability into the 21st century requires the development of quantitative methodologies to assess long-term coastal evolution in nonstationary climates (Elko et al., 2014). Coastal managers typically assess resilience to coastal hazards by tracking changes in the shoreline, a proxy or elevation contour on the beach face that exhibits significant variability on wide spatial and temporal scales (Davidson et al., 2007; Stive et al., 2002). Sophisticated process-based 3-D sediment transport modeling for shoreline prediction is still impractical at timescales of a year or more due to computational costs and the accumulation of numerical errors (e.g., Davidson et al., 2017; J. A. Roelvink, 2006), necessitating the development of approaches that strategically employ simple, computationally efficient, coastal impact models to
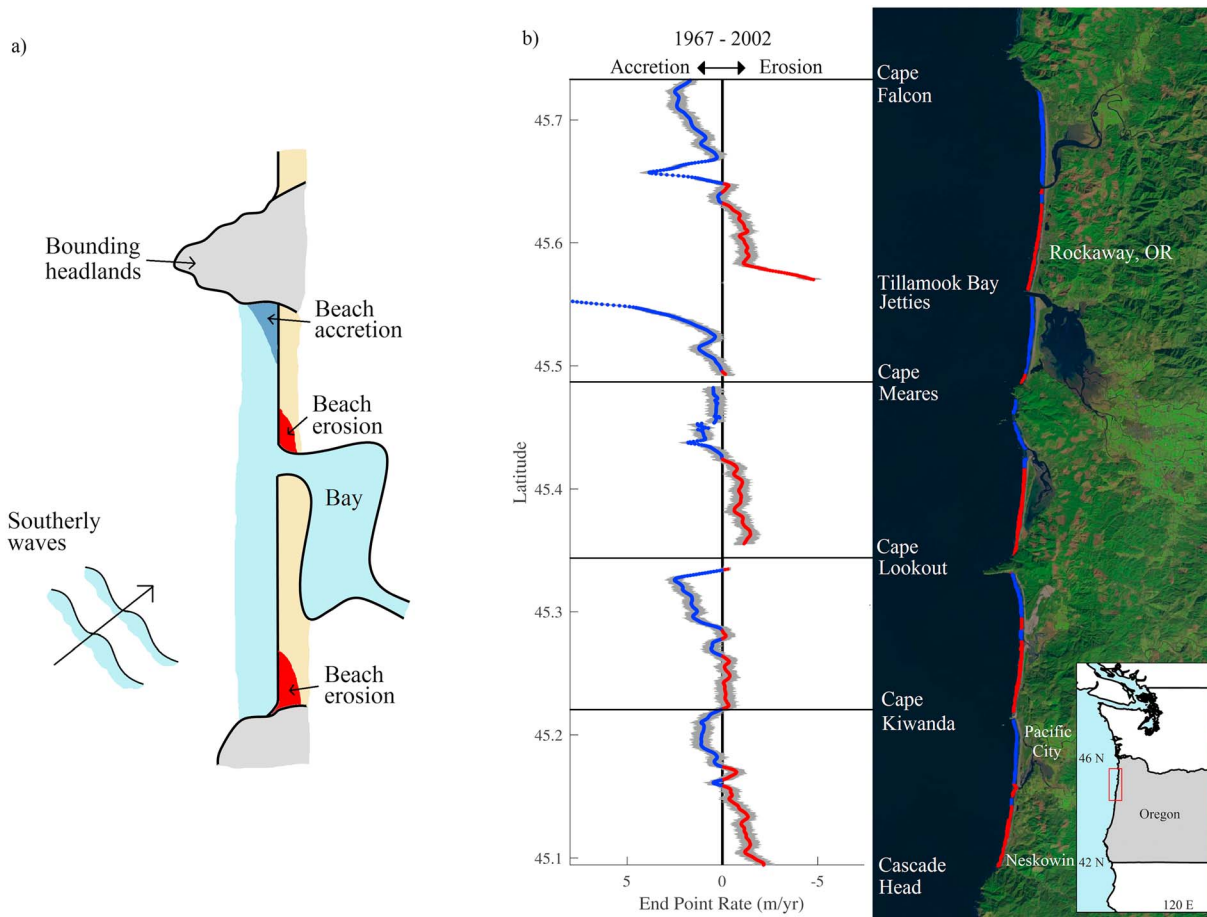
AGU
100
ADVANCING EARTH
AND SPACE SCIENCE

Journal of Geophysical Research: Earth Surface

10.1029/2018JF004689

Figure 1. (a) Drawing of typical hot spot erosion during an El Niño year (after Komar, 1998b) and (b) shoreline change between 1967 and 2002 across four different littoral cells in the north-central Oregon, U.S. coast. Blue/red denotes shoreline accretion/erosion and gray bands quantify uncertainty (after Ruggiero et al., 2013).

predict shoreline variability on timescales relevant to engineering and coastal management decisions (Ranasinghe, 2016). This study develops such a methodology, specifically creating a climate index optimized to derive continuous wave conditions for a simple shoreline evolution model driven by gradients in longshore sediment transport. Emphasis is placed on the techniques used to statistically derive wave climates and the subsequent implications for which processes and timescales dominate temporal rates of shoreline change.

The study is motivated by questions regarding the impact of climate variability on long-term coastal evolution in the Pacific Northwest (PNW) of the United States (Allan & Komar, 2006). The region is composed predominantly of dissipative beaches, ~10–50 km in length separated by intermittent headlands (Figure 1). The offshore extents of headlands typically reach deep water, effectively constraining sediment movement and creating discrete littoral cells with individual sediment budgets (Komar, 1986). Headland-bounded beaches, or embayed beaches, are a common coastal landform found throughout the world (e.g., Short & Masselink, 1999). Field studies (Harley et al., 2011; Ruiz de Alegria-Arzaburu & Masselink, 2010) and remote sensing observations (Bryan et al., 2013; Turki et al., 2013) have revealed a common geomorphic behavior whereby the embayed beach planform periodically rotates clockwise/counterclockwise. Beach rotation has been observed on multiple timescales and correlated with a variety of potential drivers, including individual storm events (Archetti & Romagnoli, 2011; Harley et al., 2014), annual oscillations due to different summer and winter wave climates (Masselink & Pattiaratchi, 2001), and interannual oscillations correlated with climate indices (e.g., El Niño-Southern Oscillation, Barnard et al., 2015; Ranasinghe et al., 2004; and North Atlantic Oscillation, T. Thomas et al., 2011). Rotations are commonly attributed to gradients in longshore transport of sediment due to changes in wave direction (Blossier et al., 2017; Short & Masselink, 1999), though recent

observations of a small embayment with large alongshore gradients in both wave exposure and sandbar location have led to additional hypotheses proposing the importance of cross-shore processes (Bryan et al., 2013; Harley et al., 2015).

Signals of shoreline rotation in the PNW have been observed during the winters of major El Niños in 1982–1983, 1997–1998, and 2015–2016 (Barnard et al., 2017; Kaminsky et al., 1998; Komar, 1986, 1998b; Peterson et al., 1990; Revell et al., 2002). Large storm waves approaching from more oblique southerly directions are believed to drive an anomalous longshore sediment transport to the north, and the gradients in longshore transport cause *hot spot* erosion north of headlands and inlet entrances (Figure 1; Komar, 1998b; Ruggiero et al., 2013). At longer timescales (interannual to multidecadal), the coast has been hypothesized to be relatively stable (Komar, 1986), with seasonal variability overwhelming any trends in shoreline evolution (10s of meters of seasonal cross-shore shoreline movement due to average significant deep water wave heights of 1.8 m with 8-s periods from west-northwest during the summer, and 3.8 m at 12 s from west-southwest during winters; Allan et al., 2003).

Recently, a comprehensive region-wide coastal change study revealed multidecadal counterclockwise rotations in multiple littoral cells in Central Oregon (Figure 1; Ruggiero et al., 2013). The long-term shoreline rotations were revealed through an endpoint rate between two shorelines obtained in the summers of 1967 and 2002, a time period which encompasses two of the three aforementioned major El Niño counterclockwise rotation events. Although widely used, trends extrapolated from historical shoreline observations through regression analysis or endpoint rates are incapable of capturing temporal variations in the change rate (i.e., trend reversals, accelerations, and decelerations; Fenster & Dolan, 1994; Ruggiero et al., 2013). Questions remain regarding the applicability of projecting the observed endpoint rate to future PNW coastal evolution. Are El Niño rotations compounding events or discrete disturbances from a long-term equilibrium? Observations of recovery following the 1982–1983 El Niño indicate that sand did not return south until 4 years after the disturbance (Peterson et al., 1990). Could the appearance of a multidecadal rotation simply be a consequence of the 2002 shoreline's proximity to the 1997 event?

Sandy coastlines naturally evolve to equilibrium with the local wave climate, with timescales to equilibrium dependent on the available wave energy and the size of the littoral cell (Elshinnawy et al., 2017; C. W. Thomas et al., 2016). The response time of the PNW's shoreline is not trivial to determine because the region experiences one of the most energetic wave climates in the world and most littoral cells are 10s of kilometers in length, therefore requiring significant sediment volume movement for discernable shoreline orientation changes. The observed multidecadal beach rotations may be the sole result of a rapid response to El Niño winters or may indicate a fundamental shift of the equilibrium shoreline orientation resulting from low frequency changes in the incident regional wave climate. Long-term multidecadal trends and oscillations in wave climates have already been detected in the region (Komar & Allan, 2008; Ruggiero, Komar, et al., 2010), with strong correlations to indices representing large-scale climate variability such as the Multivariate El Niño-Southern Oscillation Index and the Southern Annular Mode (Barnard et al., 2015). Modeling exercises have suggested that slight but persistent changes in the interannual wave climate will lead to significant shifts in coastline shape (Johnson et al., 2015; Slott et al., 2006). However, the 1967–2002 PNW endpoint rates (Ruggiero et al., 2013) include several decades during which wave observations are sparse or nonexistent, complicating any statistical assessment of observed wave climate variability.

Considerable efforts have been devoted to averting the problem of limited wave data by developing physics-based models (Booij et al., 1999; Tolman, 2002) and probabilistic techniques (e.g., Antolínez et al., 2018) to obtain realistic representations (hindcasts) of the wave energy available to force morphologic change. Several regional hindcast models are available for the PNW, including Wave Information Studies developed by the U.S. Army Corps of Engineers (Hanson et al., 2009) and the Global Ocean Wave Reanalysis 2.0 (GOW 2.0) produced by I.H. Cantabria (Perez et al., 2017). These models use dynamically downscaled wind fields beginning in 1980 to provide continuous hourly time series of wave parameters. Statistical downscaling approaches require less computational effort than numerical models and can simulate many realizations to robustly characterize variability and uncertainties resulting from the modeling framework (e.g., Antolinez et al., 2015; Rueda et al., 2017).

The purpose of this study is to reproduce plausible PNW shoreline evolutions between 1967 and 2002, including the decades without wave observations, to investigate the dominant timescales of coastal evolution. The

approach builds on recent advancements in downscaling atmospheric variability to local wave parameters (e.g., Camus, Méndez, et al., 2014). A tailor-made index was derived from sea level pressure (SLP) fields and specifically optimized to capture variability in longshore wave power. The LOngshore Sediment Transport INdex (LOST_IN) serves as a proxy for wave driven longshore sediment transport developed to predict potential offshore wave conditions (H_s, T_p, and θ) and alongshore varying nearshore equivalent conditions based on atmospheric data. This study develops a LOST_IN for littoral cells on the northern Oregon coast, which is then used to drive a simple shoreline evolution model (described in section 3) by deriving multiple extended continuous wave histories for the north-central Oregon coast (section 3). The modeled shoreline response to both interannual climatic events (El Niño) and multidecadal wave climate variability is then used to assess the dominant drivers of long-term shoreline change (section 4). Sensitivities of the modeling framework and implications for future applications of LOST_IN are then discussed (section 5) followed by concluding remarks (section 6).

2. PNW Longshore Wave Power

Although the dominant processes controlling shoreline change can vary locally depending on antecedent geology, sediment supply, and anthropogenic activity, the open coast is everywhere dynamically evolving due to the dissipation of wave energy arriving from deep water (D. Roelvink & Reniers, 2012). The flux of sediment in the longshore direction is a consequence of wave stirring and subsequent transport by the longshore current, which on dissipative and relative alongshore uniform beaches such as those in the PNW is to a first order controlled by the longshore component of wave power:

$$P_l = ECn \sin(\theta) \cos(\theta) = \frac{1}{8} \rho_w g H^2 Cn \sin(\theta) \cos(\theta), \tag{1}$$

where E is total energy, C is wave speed, n is the ratio of group to individual wave speed, and θ is angle between wave direction and shore-normal (Komar, 1998a). The longshore wave power is typically calculated at the break point after wave rays have refracted across the inner-shelf and begun to approach shore-perpendicular. However, for a relatively alongshore uniform coast, the deep water wave condition can provide a first order proxy for the direction of longshore sediment transport at a regional scale.

Instantaneous alongshore power using hourly deep water conditions (from the GOW2 hindcast) and assuming a west-facing beach is presented in Figure 2a. The summed total of every hour of northerly directed P_l during the 35-year record was 2.49×10^9 W/m, while the summed total of every hour of southerly directed P_l was -2.33×10^9 W/m. These approximately equal magnitudes support the stable coastline hypothesis (Komar, 1986). While the instantaneous alongshore power (Figure 2a) reveals the significant seasonality in the signal, the importance of interannual trends and variability are much more apparent through the integration of P_l with respect to time (cumulative longshore power, ΣP_l, Figure 2b). Steep slopes in the cumulative longshore power corresponds to consistent periods when the longshore component of wave power is directed either north (positive slopes) or south (negative slopes). El Niños produce anomalously large northerly magnitudes of cumulative longshore wave power compared to the climatological average winter (Figure 2c), in large part due to anomalous southward 10°–15° latitude shifts of Eastern North Pacific storm tracks (Peterson et al., 1990). Conversely, La Niñas are composed of southerly directed cumulative longshore wave power. The analysis in Figure 2 is based on the GOW2 hindcast through the end of 2015, and thus does not include the winter response of the major 2015–2016 El Niño (Barnard et al., 2017).

Annual fluctuations, interannual oscillations, and a long-term net northerly trend between 1980 and 2015 are all evident in Figure 2b. The interannual and long-term signals contain similar order of magnitude in ΣP_l as the El Niño signals that have previously garnered attention for hot spot erosion. In fact, during the 35-year hindcast, the summed total of hourly northerly directed P_l across all three highlighted El Niños accounts for only 11% of the total P_l (El Niño totals were taken as the sum between 1 October and 1 April the following year), which suggest that predicting future coastal evolution depends on more than just El Niño behavior. However, it should be emphasized that both P_l and ΣP_l in Figure 2 are computed with a constant shoreline orientation (North-South) and therefore do not account for the feedbacks between an evolving shoreline and the incoming wave energy. Conclusions regarding which timescales ultimately control beach rotation thus require a dynamic shoreline model accounting for the response of the beach.
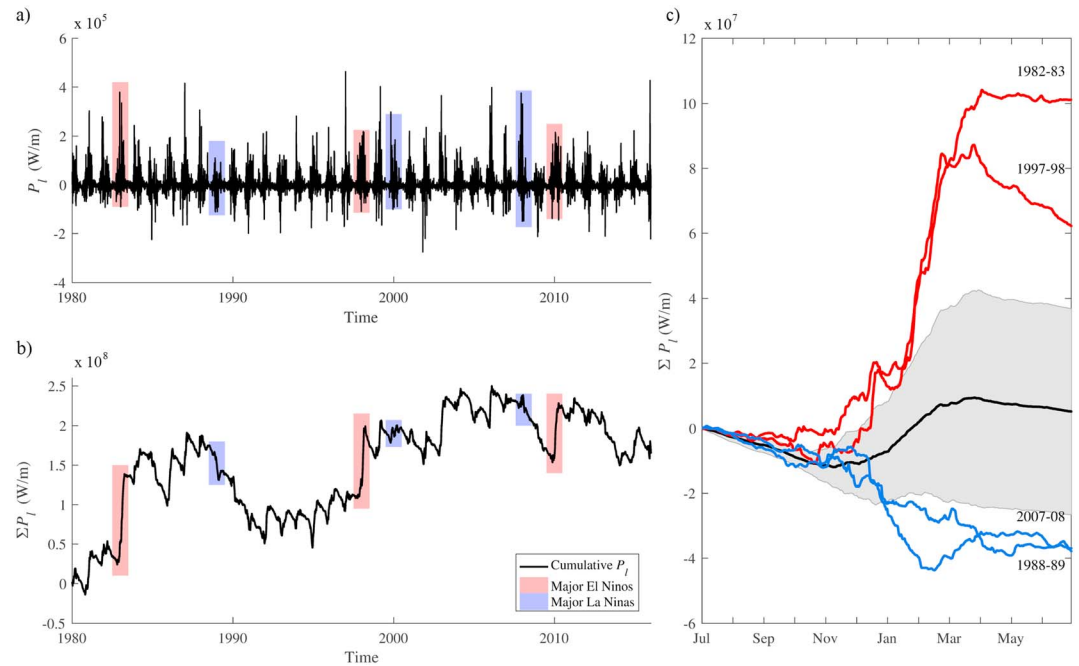
Figure 2. (a) Instantaneous longshore power calculated with deep water hindcast waves offshore of northern Oregon from 1980 to 2015 with shaded regions marking the three most significant El Niños (red) and La Niñas (blue) during the hindcast period according to the ONI index. (b) The same waves presented in (a) expressed as cumulative longshore wave power, ΣP_l, and (c) all years of ΣP_l projected to a mean (black line) and standard deviation (shaded) during a climatologic year beginning in July to capture a continuous winter response. Anomalous El Niños (red) and La Niñas (blue) are denoted to highlight their opposing winter behavior.

3. Modeling Headland-Bounded Shoreline Change

Observations of embayed beach rotation throughout the world have motivated recent efforts aimed at predicting reorientation through modeling exercises with varying degrees of complexity. Both process-based models (e.g., Daly et al., 2014; Hurst et al., 2015; Ratliff & Murray, 2014) and computationally efficient equilibrium models (Blossier et al., 2017; Turki et al., 2013) have been used to identify important external forcing processes, notably the wave direction, and internal system dynamics causing sediment exchange. For the purpose of studying littoral cells with hot spot erosion driven by gradients in longshore sediment transport, the present study uses a simple one-line model (described in section 3.1; e.g., Pelnard-Considere, 1956; Vitousek, Barnard, Limber, Erikson, et al., 2017). More complexity is introduced by creating the LOST_IN as a proxy for potential longshore sediment transport during different climatic conditions (described in section 3.2), and then deriving continuous nearshore wave conditions from the index (section 3.3.).

3.1. One-Line Shoreline Model

A simple one-line model dependent on gradients in longshore sediment transport was developed to compute shoreline change. In one-line models, cross-shore sediment exchange is typically assumed negligible (i.e., sediment volume is not transported normal to the shoreline). Instead, the cross-shore profile shape is maintained while the shoreline translates seaward/landward depending on the supply/removal of sediment by longshore sediment transport. Temporal shoreline changes are related to alongshore gradients of the sediment transport as

$$\frac{dy}{dt} = -\frac{1}{h_c}\frac{dQ_s}{dx},$$
(2)

where Q_s is the volumetric longshore sediment flux (m^3/day), h_c is the depth of closure, and x is the alongshore axis. The CERC formula was used to define Q_s as a function of the breaking wave height and the relative angle between the wave crest and the shore,
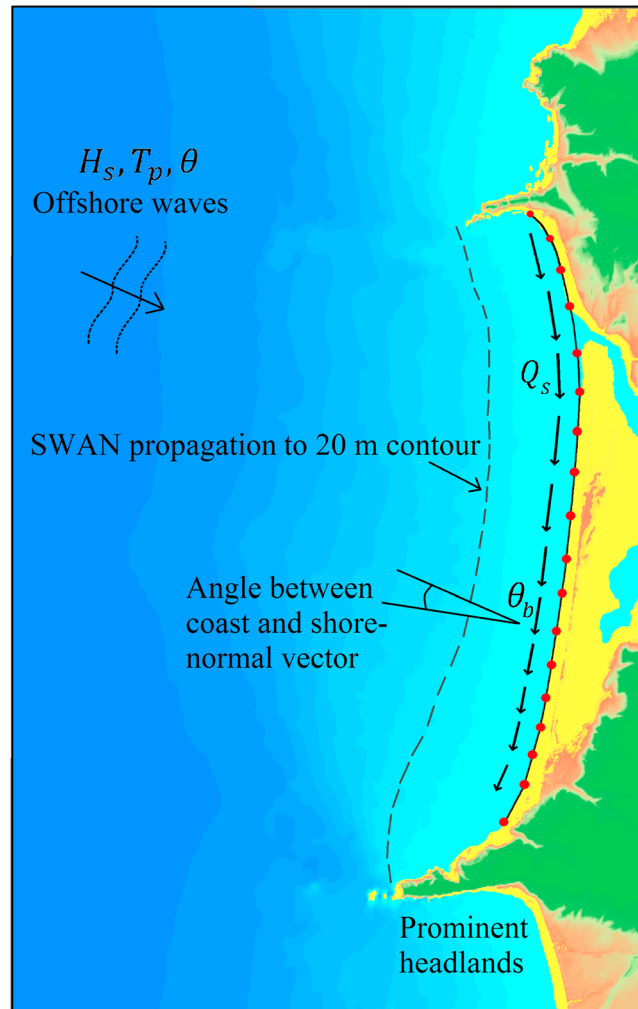
Figure 3. Schematic of one-line shoreline change model applied to a headland-bounded littoral cell typical of the Pacific Northwest. Deepwater wave conditions are propagated across the continental shelf with SWAN, extracted at the 20 m contour and linearly shoaled to individual shoreline nodes. SWAN = Simulating Waves Nearshore.

$$Q_s = K_1 H_b^{5/2} \sin^2(\theta_b - \phi), \tag{3}$$

where H_b and θ_b are the breaking wave height and direction, respectively; ϕ is the local angle of the shoreline; and K_1 is an empirical constant set to the recommended value of 0.39 m$^{1/2}$/s (Komar & Inman, 1970). It should be noted that the CERC equation is known to be sensitive to the values of K_1 (Smith et al., 2009; Figure 3) and that the many semiempirical Q_s equations available in the literature are also subject to sensitivities to calibrated coefficients (e.g., Kamphuis, 1992; Mil-Homens et al., 2013). Critiques of longshore transport formula suggest that values provided by such predictions should only be considered as order-of-magnitude accuracy (Pilkey & Cooper, 2002). This order of magnitude accuracy was considered acceptable in this study for the broader intention of investigating dominant trends of shoreline variability as opposed to replicating exact magnitudes for engineering applications.

Due to the relatively large scale of PNW littoral cells (O[10s of kilometers]), the shoreline model is built to account for alongshore nonuniformity of the nearshore wave field resulting from shoaling and refraction during wave propagation across the shelf bathymetry and in the vicinity of headlands. A previously developed library of dynamic wave transformations from deep water to the 20 m depth contour by the numerical model Simulating Waves Nearshore (SWAN, Booij et al., 1999) was used to derive alongshore varying wave conditions and thus alongshore varying Q_s at shoreline nodes spaced 250 m apart. Spatial gradients of Q_s were

then derived numerically with zero flux boundary conditions imposed at adjacent headlands and jetties to obtain spatially varying $\partial y/\partial t$ in an iterative fashion. As a result, the modeled shoreline evolution is fundamentally dependent on the chronological order of the waves and the antecedent shoreline configuration.

The lookup table of SWAN runs covered the full range of potential wave conditions (9 H_s cases, 11 T_p cases, 13 θ cases, and 2 water level cases for a total of 2,184 SWAN model runs forced by Joint North Sea Wave Project spectrums along the offshore boundary; Allan et al., 2015). The grid resolution was 100×100 m spanning 139 km in the alongshore and extending 72 km to deep water off the Oregon continental shelf with an outer boundary located at the GOW2 hindcast in Figure 2. No model calibration was performed but validation and sensitivities to various processes such as bottom friction were performed at multiple inner-shelf National Data Buoy Center (NDBC) buoys (see Allan et al., 2015, for further details regarding the SWAN model configuration). The lookup table facilitates the quick creation of synthetic time series of alongshore varying nearshore conditions based on an offshore time series of wave triplets. Fifty years of offshore waves can be turned into 10s of kilometers of unique nearshore nodes on the order of minutes with an efficient interpolation scheme across the library. This provides the shoreline model with considerable flexibility, allowing for Monte Carlo simulation of the shoreline change due to different time series of offshore conditions.

Although the SWAN model could have provided breaking wave conditions relevant to the CERC equation, those conditions are only applicable to the bathymetry from 2010 used by Allan et al. (2015) to develop the lookup table. A base assumption of this study is that the shoreline translated seaward and landward over multiple decades, which alters the nearshore bathymetry from the toe of the profile through the transient sandbars and the edge of the wave break point in the surf zone. Instead, nearshore conditions are derived with SWAN at the 20-m depth contour after transforming across the continental shelf and then further shoaled and refracted with linear Airy theory to an assumed break point at the wave height to water depth ratio of 0.78.

The depth of closure, h_c, controls how much of the cross-shore profile sediment volume is distributed across, with larger h_c values resulting in less shoreline translation for the same volume of transported sediment. The 12-m contour is used for h_c in this study based on previous observations of the depths to which PNW beach profiles actively evolve (Ruggiero et al., 1998). The one-line model is closed by conserving sediment volumes and creating impermeable boundary conditions at bounding headlands. The assumption of negligible net sediment inputs/sinks is justified by the relatively straightforward sediment budgets of most north-central Oregon littoral cells. Each cell is typically composed of largely relict sediments with small quantities contributed by modern sea-cliff erosion and streams and small quantities removed by estuary infilling (Komar, 1998b; Ruggiero, Buijsman, et al., 2010). The potential for sediment bypassing at headlands is assumed negligible for this study but is still an open question in the PNW region at long timescales.

3.2. Creating LOST_IN

Continuous wave conditions for time periods prior to available hindcasts must be derived before the one-line model can reproduce the observed shoreline signal starting in 1967. Dynamical wave-generation modeling approaches use surface wind stress to produce wave sea states, with forcing typically provided by atmospheric models at some elevation above the ocean (i.e., winds at 10 m). Subsequent interpolations and parameterizations for friction and growth of swell waves are applied with a number of user decisions for calibration (e.g., WAVEWATCH III Development Group (WW3DG), 2016). In contrast to dynamic downscaling techniques, the approach developed in this study uses a statistical downscaling methodology to identify atmospheric conditions most relevant to longshore sediment transport in the PNW. We employ a fundamental assumption that waves are correlated to the spatial and temporal variability of SLP. While this assumption certainly has uncertainty, it is intended to avoid the cascading uncertainty associated with both atmospheric and wave model parameterizations that is difficult to quantify with respect to space and time. The fundamental relationship between ocean waves and SLP fields has been utilized by a number of studies to investigate seasonal wave height variability (Wang et al., 2012), as indicators for weather-type classifications of wave climates (Antolinez et al., 2015; Camus, Menéndez, et al., 2014) and as predictors for future wave climates (Casas-Prat et al., 2014; Perez et al., 2015; Wang et al., 2004).

LOST_IN is derived from SLP fields and the squared gradients of those fields obtained from National Centers for Environmental Prediction (NCEP)/National Center for Atmospheric Research (NCAR)'s Reanalysis 1 with
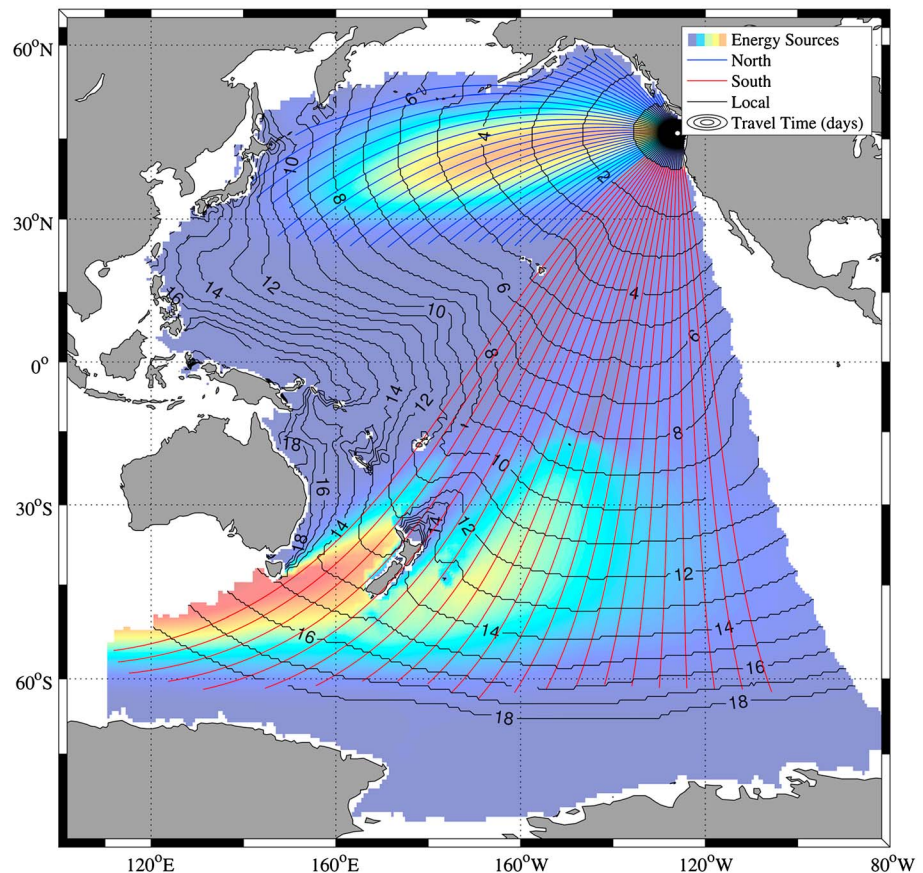
Figure 4. The spatial distribution of wave energy produced in the Pacific Ocean with the potential to reach the coast of northwest Oregon is denoted by relative color (red = more energy, blue = less) as identified by Evaluation of Source and Travel-time of wave Energy reaching a Local Area (Perez et al., 2014). Numbered contours identify the number of days it takes waves from a particular part of the ocean to travel to Oregon. Great circle arcs emanating from Oregon denote regions of North Pacific swell (blue), South Pacific swell (red), and local wind wave generation (black), with the end of the lines denoting where 99% of the energy is produced.

temporal coverage every 6 hr since 1948 on a global grid with 2.5° resolution (Kalnay et al., 1996). While statistical models can fundamentally be sensitive to the number of nodes used to define relationships, higher resolution than that provided by the NCEP/NCAR Reanalysis was deemed unnecessary in terms of statistical significance as well as dynamically uncertain in terms of relying on high resolution weather products in years prior to quality satellite observations. SLPs for LOST_IN are only considered in regions which generate wave energy directed toward the PNW coast (Hegermiller et al., 2017). The wave source regions and travel times are identified using Evaluation of Source and Travel-time of wave Energy reaching a Local Area (ESTELA) (Perez et al., 2014), which tracks wave generation directed at the GOW2 node in deep water off of the PNW coast (45.893°N, 125.819°W, colocated with NDBC buoy 46089). ESTELA reveals significant wave energy generation associated with extratropical cyclones in the North Pacific above 30°N and in the South Pacific from low pressure systems circulating the Southern Ocean (Figure 4). The two regions are considered separately in further analysis as representing the swell components from the North and South Pacific Ocean.

Less than 1% of the wave energy reaching Oregon is generated in regions beyond the boundaries shown in Figure 4. The average travel time for waves is calculated along each arc and the single day travel time contour is used to define a third region representing the generation of local sea states (Figure 4). The travel time from the farthest extent of each swell region is 18 days, indicating that the wave spectrum arriving on any given day may be a combined function of distinctly different SLP fields occurring during as much as a 2- to 3-week window. A method proposed by Hegermiller et al. (2017) is used to construct an atmospheric predictor field,
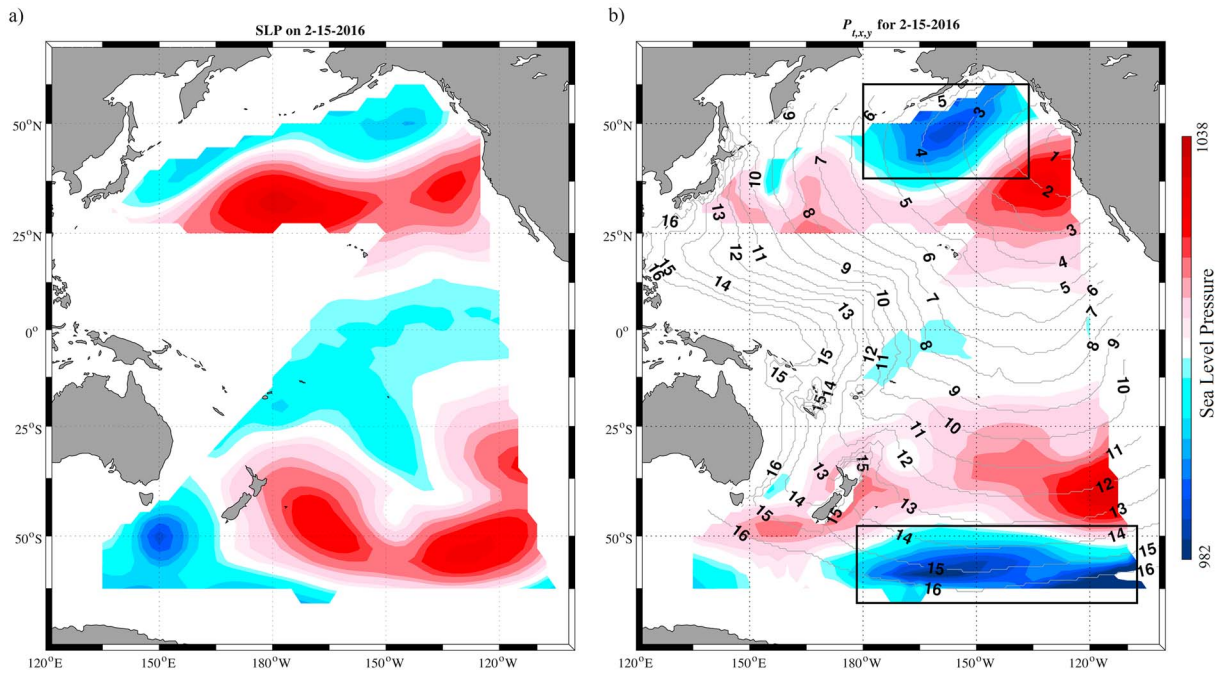
Figure 5. (a) The SLP field for 15 February 2016 compared to (b) the atmospheric predictor built for the same day but considering the memory of the system by utilizing SLP fields from up to 16 days prior to 15 February. Black boxes in (b) indicate low pressure systems that generated swell on different days in the North (10–12 February) and South Pacific (31 January to 2 February) but that arrived to Oregon at the same time (the fifteenth). Gray contours in (b) represent the average number of days for a wave generated at that location to travel to Oregon. SLP = sea level pressure.

$P_{t, x, y}$, such that spatially distant regions of the ocean are defined by SLP fields corresponding to lagged times. The example provided in Figure 5 demonstrates how $P_{t, x, y}$ may deviate from the instantaneous SLP field. A large low pressure system was located south of the Aleutian Islands between 10 and 12 February 2016, generating swell waves that arrived to Oregon on the fifteenth. Although the instantaneous SLP field for 15 February does not contain the deep low pressure as a potential wave generator (Figure 5a), the $P_{t, x, y}$ field includes the memory of the system and retains the influence of the low pressure on the instantaneous wave climate (Figure 5b). Deviations from the instantaneous SLP field are much greater at farther contours. For instance, the strong high pressure in the central north Pacific on the fifteenth (Figure 5a) was not present 6 to 8 days earlier (Figure 5b), and a large low pressure system was present 2 weeks earlier in the South Pacific that may have generated swell waves relevant to northwest Oregon on the fifteenth (Figure 5b).

At this step, the user may make a choice of the timescale of climate resolution by averaging $P_{t, x, y}$ fields to daily or monthly fields. Dominant modes of atmospheric variability are then identified through a principle component analysis (PCA) of the $P_{t, x, y}$ fields, which quantitatively identifies common spatial patterns (empirical orthogonal functions, EOFs, function of space) and the temporal coefficients of those spatial patterns (PCs, function of time). A separate PCA is performed for each region of wave generation (north, south, and local). Physically, the decomposition identifies the locations and persistence of low and high pressure systems throughout the Pacific Ocean that are relevant to the overall wave climate of north-central Oregon (i.e., the location of interest in this study).

However, not all atmospheric conditions generate wave conditions necessarily relevant for longshore sediment transport at this study site. Identifying the atmospheric conditions that contribute most to longshore sediment transport in north-central Oregon is performed by statistically associating the temporal variability of each EOF pattern with the cumulative $\sum P_l$ time series at monthly scale between 1980 and 2015 (Camus, Méndez, et al., 2014). A multivariate regression model is used to linearly combine statistically significant EOFs, each with a temporally constant coefficient. Building the regression model is an iterative process, first identifying which PC time series is best correlated with the time series of monthly $\sum P_l$, then linearly combining the first identified PC with every other PC to determine which pair-wise combination
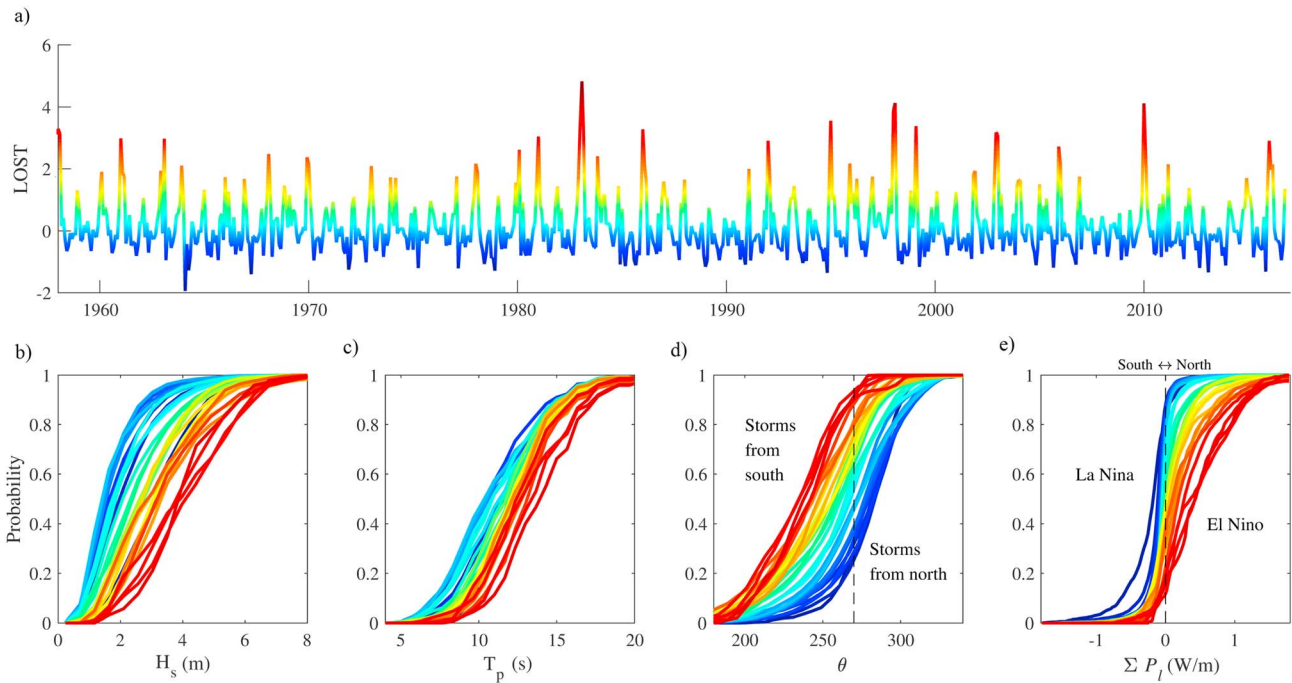
Figure 6. (a) Complete time series of LOST_IN_Oregon computed at monthly scale. Color ramp highlights variability of LOST_IN to denote which months' data are binned together to create the colored distributions of (b) wave height, H_s; (c) peak period, T_p; (d) mean direction, ϕ; and (e) alongshore wave power ΣP_l. LOST_IN = Longshore Sediment Transport Index.

explains the most variance in the ΣP_l time series. The addition of more PCs to the index is continued until a Fisher's test determines that the improvement of the model is not significant beyond the added degrees of freedom,

$$LOST_{IN(t)} = \Sigma CR_n \times PC_n(t), \tag{4}$$

where CR is a coefficient of regression and n is an index of the EOFs identified by the iterative process. The coefficient is a free parameter in the model that is held constant through time.

The resulting tailor-made cumulative index, LOST_IN_Oregon, is specifically constructed to identify which spatial patterns of atmospheric variability generate waves that have a longshore component of wave power along the north-central Oregon coast. The index results in a continuous time series, extending records of longshore wave power to encompass times without wave observations because the statistical model derived by equation (4) is effectively a predictive equation dependent on only the atmospheric $P_{t, x, y}$ fields. Essentially, the methodology is able to identify any atmospheric pattern in the Pacific Ocean and predict the resulting local longshore wave power at the study site. An example of LOST_IN_Oregon formed with monthly averaged $P_{t, x, y}$ fields is provided in Figure 6a. Positive (negative) values of LOST_IN_Oregon indicate northerly (southerly) longshore sediment transport, with values around zero indicating waves that are either small or arriving perpendicular to the shoreline orientation. The most common atmospheric patterns, or the EOFs that explain the greatest variability in the PCA, do not necessarily contribute the most to LOST_IN_Oregon because the nonlinear relationship with wave angle in equation (1) drives a preferential choosing of atmospheric patterns correlated with weather systems approaching from oblique angles. For the example provided in Figure 6, the first five EOFs chosen by the multivariate regression model in order of importance, were the first, tenth, third, thirteenth, and sixteenth, resulting in a total 36 out of 2,792 possible EOFs used to create LOST_IN_Oregon.

3.3. Time Series Simulation

LOST_IN indicates the obliquity of deep water waves given an offshore climate pattern, but does not provide specific wave parameter triplets (H_s, T_p, and θ) nor alongshore varying breaking wave conditions necessary to
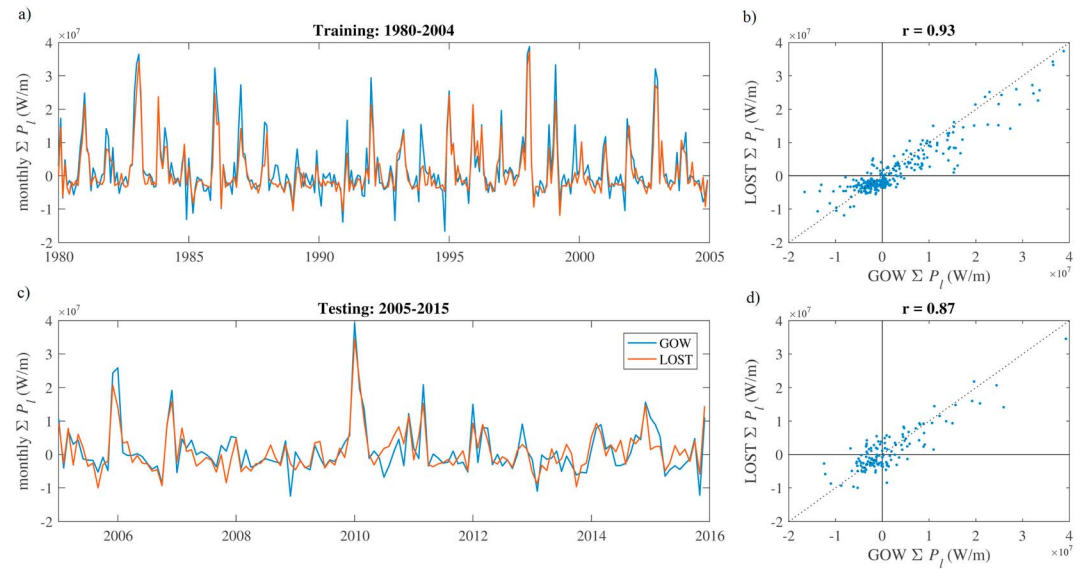
Figure 7. (a) Training of the LOST_IN methodology on monthly ΣP_l from GOW 2.0 between 1980 and 2004 with (b) one-to-one comparison of ΣP_l after simulating wave triplets. (c) Time series and (d) one-to-one comparison of a testing time period from 2005 to 2015 during which the methodology is only provided atmospheric data. GOW 2.0 = Global Ocean Wave Reanalysis 2.0; LOST_IN = Longshore Sediment Transport Index.

drive the one-line model described in section 3.1. A two-step hybrid method is developed to determine inputs for the shoreline model, first through a probabilistic step to obtain deep water waves and second through a dynamic step to obtain nearshore wave conditions.

Deep water wave triplets are determined by associating specific ranges of LOST_IN values to probability distributions for wave parameters from the observed (hindcast) record. A one-dimensional K-means algorithm is used to bin the index into uneven bin intervals, which ensures that each bin contains enough wave conditions from a training time period to develop well-defined marginal and joint probability distributions. The resulting distributions reveal distinct clusters within the wave climate (Figures 6b–6d). Large storm waves approaching from steep southerly (northerly) directions form joint distributions representative of the positive (negative) extreme of the index (Figure 6e). Joint probabilities of H_s, T_p, and θ are defined using student t copulas with empirical distributions to ensure realistic longshore wave power approaches the coast from the appropriate angles for each atmospheric condition.

Any particular LOST_IN bin is thus assumed to represent a generalized spatial climate pattern on user defined timescale (i.e., daily and monthly), and during the occurrence of such a climate pattern a range of potential offshore wave conditions could be generated (the copula distributions). Time series of nearshore wave conditions are then simulated by randomly selecting offshore wave triplets from the appropriate LOST_IN bin copula (e.g., Serafin & Ruggiero, 2014), and subsequently generating alongshore varying nearshore wave conditions via the dynamic lookup table. Random selection from the copula to drive the shoreline model is performed at the hourly scale, which is a high enough sampling rate that the shoreline model is effectively driven by a particular climate's distribution of wave conditions (i.e., randomly selecting ~720-hourly conditions during a month reproduces simulated wave probability distributions representative of all previous observed conditions during the climate). This technique is also beneficial for the stability of the one-line model, as it prevents random selection of an extreme wave from being applied for too long and causing unrealistic dy/dt (i.e., an entire 24 hr of steeply approaching peak storm waves).

Figure 7 demonstrates training and testing of hourly simulated waves derived from the monthly LOST_IN_Oregon time series presented in Figure 6. In this example, a cumulative monthly ΣP_l is obtained from all randomly selected hourly wave conditions during that month and compared to the observed monthly ΣP_l derived from hourly GOW 2.0 conditions. The optimum number of monthly LOST_IN bins for the Oregon coast was determined to be 30 by an iterative process seeking the strongest correlation between observed and simulated ΣP_l. Sensitivity analyses have shown that the correlation during both training and

testing time periods is dependent on the length of the training. As expected, a longer training period provides the model with a greater variety of atmospheric conditions which results in a better separation of the wave climate. Training during a time period with at least one major El Niño is particularly important because the atmospheric conditions during these events are anomalous compared to other climatic conditions. Note that the example provided in Figure 7 contains the 1982–1983 and 1997–1998 El Niño events in the training period and therefore the approach is able to replicate the cumulative longshore wave power during the major 2009–2010 event with significant skill.

4. Application to a North-Central Oregon Littoral Cell

As demonstrated in Figure 1, the littoral cells in north-central Oregon displayed consistent counterclockwise shoreline rotations between 1967 and 2002. Here we focus on a 17 km long beach from Rockaway to Manzanita as a representative stretch of the Oregon coast. The northern boundary of this cell is Cape Falcon, while the southern boundary of the model is the jettied entrance to Tillamook Bay (Figure 1) which effectively serves as a headland limiting sediment transport to the south. The town of Rockaway, OR (denoted in Figure 1), is located along the southern portion of the cell, with much of the town eroding faster than -1 m/year and localized rates of erosion reaching -3 m/year (Figures 8a and 8b; Ruggiero et al., 2013). Small, unmaintained jetties approximately 200 m in length, at the entrance of Nehalem Bay, are responsible for a locally large accretion signal at ~10 km in Figure 8b. However, for simplicity, the shoreline was smoothed to remove the inlet and neglect the localized effect because the surf zone is often wider than the offshore extent of these jetties and contextual evidence suggests complete bypassing of the littoral drift. The shoreline was initiated with an equilibrium shoreline, the implications of which are described more in depth in section 5.1.

4.1. Shoreline Change Results

The one-line model was initiated in 1957, because of inhomogeneities in the NCEP/NCAR reanalysis prior to this year (Kistler et al., 2001), and run through September 2017 using randomly sampled waves derived from the LOST_IN methodology for the entire time frame. Shorelines from the model were extracted for dates corresponding to the 1967 and 2002 data sets in Ruggiero et al. (2013) to produce the modeled endpoint rate shown in Figure 8c, which exhibits a similar counterclockwise rotation to that observed. The ability of the one-line model to replicate long-term littoral cell behavior supports the hypothesis that longshore sediment transport is the dominant process producing the multidecadal rotations in Oregon. The modeled rotations are largely limited to the 5 km adjacent to each boundary of the littoral cell, with the central 10 km exhibiting change rates close to zero between these two dates. The CERC equation was not calibrated for this shoreline change hindcast as the intention was to derive relative trends and explore dominant timescales of change. However, greater (lower) K_1 coefficients in the CERC equation result in more (less) of the littoral cell's central shoreline experiencing rotational behavior due to the diffusion of stronger (weaker) gradients into the rest of the shoreline domain. This process is nonlinear with respect to changing magnitudes of K_1, but the same general counterclockwise rotation was observed regardless of the coefficient used.

The modeled multidecadal rotation also provides confidence that the one-line model may be realistically simulating shoreline behavior at interannual timescales. This notion is supported by a direct comparison to shorelines extracted from seasonal beach profile surveys. Cross-shore profile data have been collected with RTK GPS approximately quarterly since October 2004, providing 46 different dates for assessing temporal behavior (Allan & Hart, 2008). The surveyed data inherently contain all nearshore processes acting on the beach, including cross-shore exchanges of sediment between the sandbar and beach face occurring at seasonal scale. The one-line modeling framework presented in this work assumes this process is essentially noise superimposed on the long-term trends, thus shorelines for comparison to the model are extracted at the 3.7 m contour relative to NAVD88, a beach level considered to be more indicative of long-term coastal evolution because it is typically above the region of highly mobile intertidal sandbars and seasonal berm development (Cohn et al., 2017). Two separate transects from the central and southern portions of the Rockaway littoral cell are compared in Figure 9 with the beach profile data set. The data have been transformed to model coordinates by setting the first observation to be the same position as the modeled shoreline at that particular date.
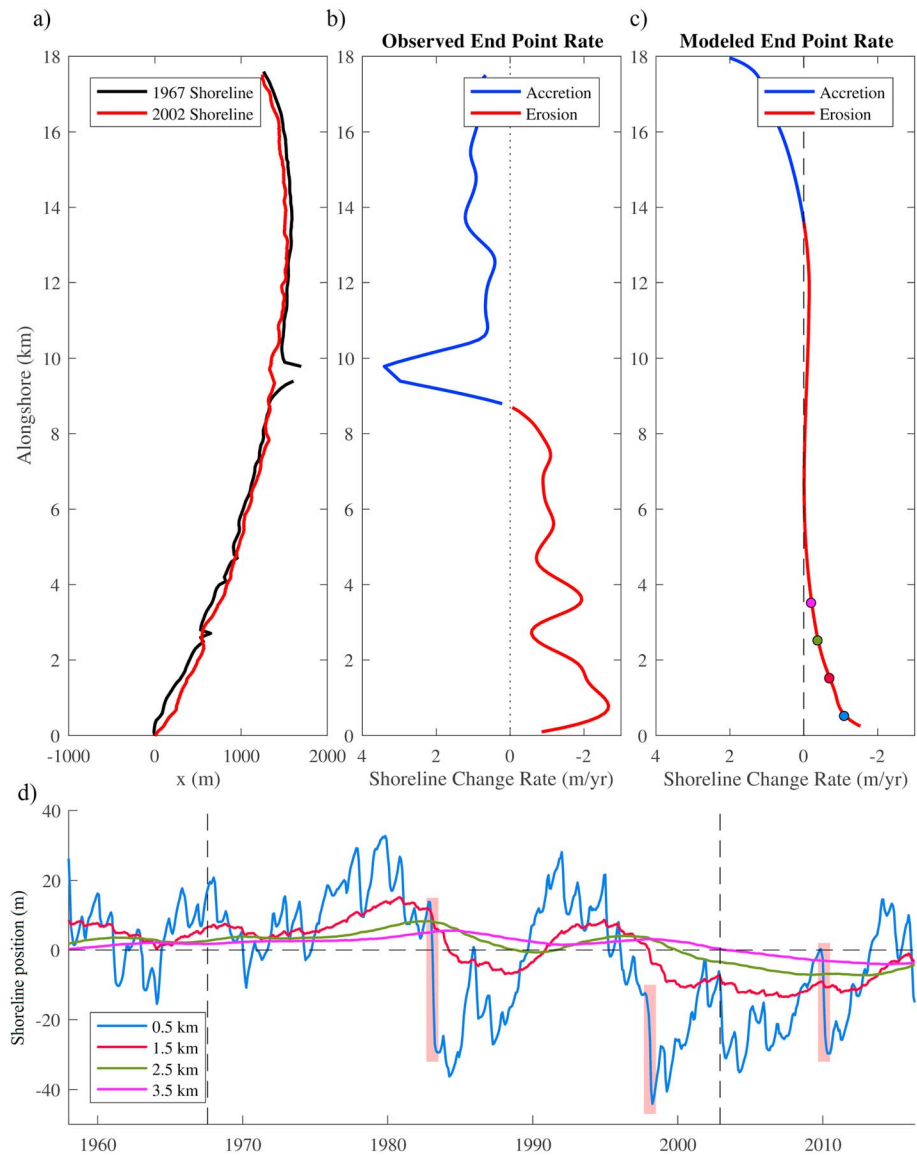
Figure 8. (a) The observed shorelines for the Rockaway littoral cell in 1967 and 2002 and (b) the corresponding endpoint rate shoreline change signal between the two shorelines. (c) The endpoint rate produced by extracting shorelines from the model on the same corresponding dates and (d) the temporal behavior of several shoreline nodes at select distances from the southern boundary with large El Niños highlighted by red shading (alongshore location also noted by corresponding color in (c)).

Model results exhibit comparable behavior to observations at the southernmost transect in both magnitude and timing of shoreline movement during the 13 years of available data. The model successfully predicts the general observed trend of accretion from approximately 2006 to the late 2000s, the erosion during the El Niño Modoki winter of 2009–2010, and the following 6 years of general accretion before another El Niño induced erosion event in 2015–2016 (Figure 10b). It is notable that behavior on interannual timescales appears to be predicted with reasonable skill (i.e., erosion and accretion between 2015 and 2017).

Model results and data also display general agreement in the middle of the littoral cell in terms of the overall accretion pattern during the entire time period. However, the model does not capture the magnitude of the observed accretion. This discrepancy could be either due to uncertainties in the modeling framework or due to unmodeled natural processes. Previous studies in the region have documented cross-shore feeding from the shoreface to the beach (Ruggiero, Buijsman, et al., 2010), a process which could be contributing to the long-term evolution of the Rockaway littoral cell but is unaccounted for in the present version of the one-
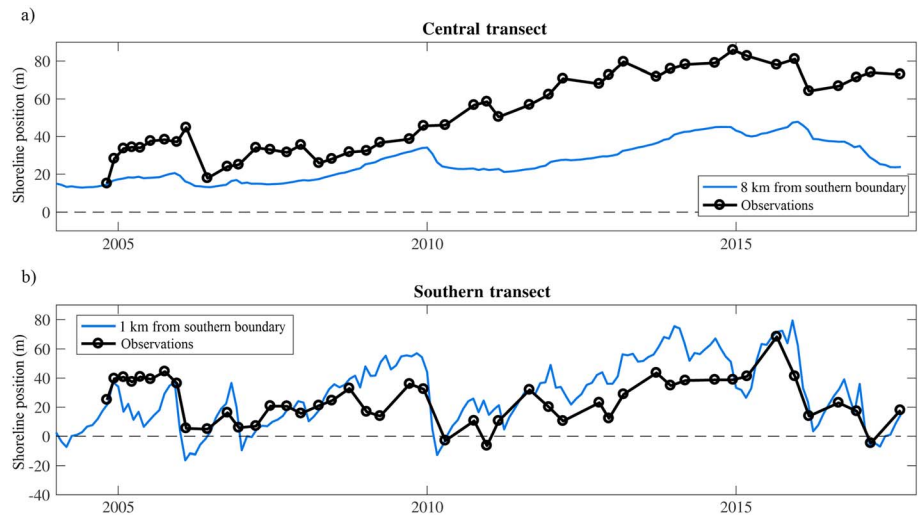
Figure 9. Temporal comparison of the 3.7 m contour extracted from discrete beach profile surveys (black dots) and continuous shoreline positions from the one-line model for (a) a shoreline node in the middle of the cell and (b) a shoreline node near the southern extremity.

line model. The simplicity of using an alongshore constant $K_1 = 0.39$ in the CERC equation could also be contributing to the under prediction of beach response. However, the Shoreline Protection Manual's recommended value of 0.39 has been previously critiqued as resulting in an over prediction of quality data sets (Bayram et al., 2007; Smith et al., 2009). Greater K_1 coefficients produced larger shoreline change signal in the middle of the domain, but also negatively affected comparisons at the ends of the domain. There is the potential that calibrating an effective K_1 for each transect in the alongshore may have
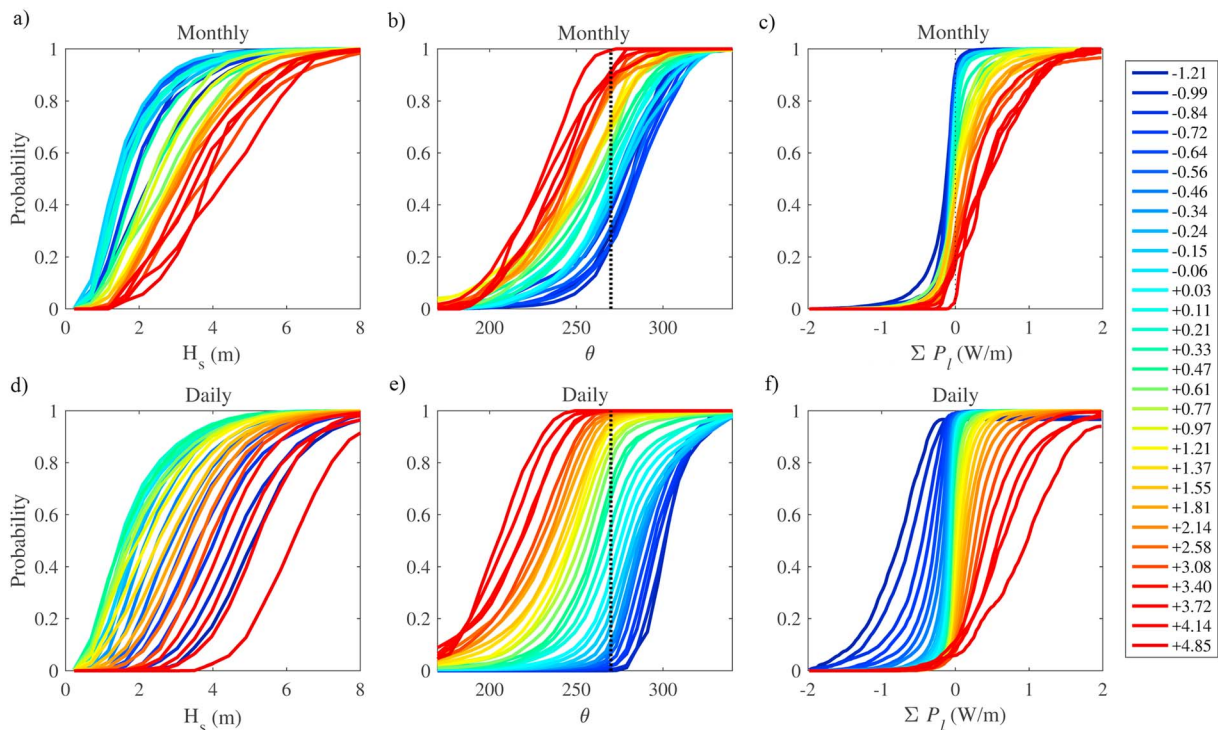

Figure 10. (a) Significant wave height, H_s; (b) mean direction, θ; and (c) ΣP_l distributions for 30 bins composed of monthly Longshore Sediment Transport Index data (similar to Figures 6b, 6d, and 6e). (d), (e), and (f) are distributions of H_s, θ, and ΣP_l, respectively, for distributions composed of daily Longshore Sediment Transport Index data.

produced result of closer magnitude to the observations, but such extensive calibration was beyond the scope of this investigation.

Despite the potential effects of cross-shore processes, the direct comparison with survey data indicates that the model provides insight to shoreline behavior between 1967 and 2002. Seasonal, interannual, and multi-decadal signals are all apparent when the shoreline position of specific alongshore locations are tracked through time (Figure 8d). The convention in Figure 8 is such that positive (negative) values are shoreline advance (retreat) relative to the initial shoreline position, which for the four locations provided at the southern end of the littoral cell corresponds to clockwise (counterclockwise) rotations. The shoreline node 0.5 km from the southern boundary (blue) exhibits the greatest variance, including the greatest retreat during El Niño winters when hot spot erosion occurs due to anomalous waves from the south. However, the simulation suggests that the interannual to multidecadal oscillations have a larger effect on whether the beach is in an eroded or accreted state relative to the initial conditions. For instance, the hot spot erosion during the 1997 El Niño produced the most landward shoreline in the simulation, but the El Niño accounts for less than 40% of the total retreat observed between 1991 and 1997 due to the cumulative erosional trend during the 5 years preceding the El Niño. A similar erosional trend began prior to the 1982–1983 El Niño, indicating that littoral cell rotations in the PNW are not simply a consequence of anomalous sediment movement during individual El Niño winters followed by subsequent reorientation, but rather dominated by decadal scale oscillations.

The modeled shoreline at 1.5 km from the southern boundary (red) exhibits decadal oscillations with less intra-annual variance (Figure 8d) than immediately adjacent to the boundary. Modeled shoreline variability at 2.5 (green) and 3.5 km (purple) from the boundary are dominated by decadal timescales with no interannual or intra-annual variance. Model results at these locations show a general trend of clockwise rotation from 1958 to approximately 1980 and then counterclockwise rotation to the present. The reversal time between clockwise and counterclockwise rotations also appears to be a function of distance from the jetty, as the most accreted location of each node occurs across a lagged 5-year window between 1980 and 1985. This behavior provides an indication for the response time of the beach, suggesting that the gradients in longshore transport driving rotations propagate in the alongshore on interannual timescales.

The interannual variability in the shoreline behavior can significantly alter the relevance of any linear shoreline change rate (endpoint or regression) obtained from historical data and projected into the future. Such change rates are aliasing an oscillating signal and tell a different story depending on when the observation of shoreline position is made. The largest potential endpoint rate for the extremities of the littoral cell (between the winter of 1979 and summer of 1985) results in shoreline change rates 8× greater than the endpoint rate reported on between 1967 and 2002. However, an endpoint rate from 1985–1992 results in comparable magnitude change rates but in the opposite direction of rotation, while endpoint rates computed between 1972–1995 and 1965–2016 give change rates close to zero and would indicate no rotation of the beach.

5. Discussion

5.1. Model Sensitivity

5.1.1. Initial Shoreline

Initiating the shoreline model with the measured shoreline position in 1967 produced unrealistic shoreline change trends on the order of ~10 m/year. Fundamentally, the presence of any gradient in longshore transport is a function of the disequilibrium between the shoreline configuration and the wave condition (Elshinnawy et al., 2017). In natural systems with closed sediment budgets, a consistent shoreline change is the result of an inherited orientation reorganizing to new wave conditions. Therefore, the quality of any modeled shoreline change signal is dependent on both the quality of the initial shoreline position and the quality of the wave information. If an observed (true) shoreline is used in the model and the modeled wave climate is biased slightly from the true wave direction, or if the wave transformation dynamics between the offshore and the shoreline are not represented correctly, then the subsequent modeled shoreline evolution is not representative of true shoreline evolution but simply the model attempting to reach the equilibrium shoreline orientation specific to that wave climate. The resulting gradients in sediment transport at any single time step may be very small, but the cumulative effect of decades of biased waves would appear in the one-line model results as a multidecadal shoreline rotation.

The one-line model results in section 4 were initialized from an equilibrium shoreline specific to the Rockaway littoral cell SWAN lookup tables to ensure that the modeled multidecadal rotation was not simply a reorientation of the beach to biases present in the SWAN derived wave climate. To achieve an equilibrium shoreline, the one-line model was first initialized with a straight shoreline subject to a synthetic climatological wave climate. The hindcast wave climate was binned into monthly distributions (i.e., all January waves grouped to a single distribution, and all Februaries), and the synthetic wave climate consisted of a time series of hourly wave conditions created by randomly selecting from the appropriate month during simulations that were run until annual shoreline change in the one-line model was negligible. Simulations took on the order of 100s of years to reach shoreline orientation equilibrium, and negligible change was determined when consecutive December shorelines in the model were less than 1 meter different at all model nodes. The synthetic climate used to generate the initial equilibrium shoreline effectively removed decadal and interannual oscillations in the wave climate as well as the impulsive response caused by El Niños, but retained the mean monthly wave climate to produce a seasonal oscillation between summer and winter to create the concavity of the embayed beach. The same equilibrium shoreline orientation was obtained by evolving an initially straight shoreline and by evolving the observed 1967 shoreline (Ruggiero et al., 2013), suggesting that the methodology described above produces an equilibrium shoreline purely dependent on the incident SWAN wave climate.

Fitting a linear regression to the equilibrium shoreline suggest a 1.5° more westward facing beach compared to the true shoreline. This difference is relatively small when considered within the context of a 35° seasonal shift in wave direction, but the cumulative effect of this small difference in angle along the 17 km long littoral cell modeled here is an ~450-m difference at the extreme ends of the beach, which was likely the cause of the unrealistic shoreline change rates when initiating the model with the true 1967 shoreline. It is possible that SWAN may not be capturing all physical processes affecting wave propagation. The 1.5° shoreline angle offset could also simply be a consequence of discretizing the wave spectrum into directional bins (5° bins).

5.1.2. Temporal Averaging of LOST_IN

Climate indices are typically expressed as either daily or monthly values. The temporal resolution of LOST_IN is an arbitrary user-defined parameter controlled by the time period over which SLP fields are averaged. The probability distributions of potential wave conditions derived from daily versus monthly LOST_IN follow the same general trend highlighted in Figure 6, separating the wave climate into conditions approaching from steep angles with large waves. Daily distributions capture noticeably greater variability in wave directions than the monthly bins, and reveal several wave height distributions almost entirely above 4 m (Figure 10). These bins are identifying specific atmospheric conditions related to storms on the order of a day to a week in length that are otherwise smoothed when applying LOST_IN at the monthly timescale. This smoothing is most likely the dominant mechanism leading to some of the poorly simulated large southerly longshore fluxes in the monthly example provided in Figure 7. Closer analysis revealed that these southerly directed fluxes are due to storm events less than 3 days in length occurring during the transition from summer to fall. The rest of the month is composed of summer-like conditions concealing the strong longshore flux conditions at the tail of tri-variate copula distributions dominated by calm waves. The daily temporal average is thus capable of resolving the individual meteorological events, while the monthly average is more representative of the large-scale climate variability.

The decision for what timescale to use in developing LOST_IN ultimately depends on the desired processes being resolved. Figure 11a provides a comparison of $\sum P_l$ derived from 100 simulations of daily LOST_IN and 100 simulations of monthly LOST_IN between June 2015 and June 2017. Randomly sampling from the same copula of wave conditions throughout an entire month neglects the intramonthly chronology of waves and produces a consistent linear trend for $\sum P_l$ within each month (red envelope in Figure 11a). Such an assumption is unrealistic with respect to the chronology of individual weather systems, but the overall correlation between modeled $\sum P_l$ and hindcast $\sum P_l$ between 1979 and 2015 is better for monthly LOST_IN ($R = 0.92$; Figure 11b) than for daily LOST ($R = 0.82$; Figure 11c). The reduced correlation at the daily scale is a function of daily LOST_IN resolving greater variance in both the atmosphere (less smoothing of SLP fields) and longshore wave power (daily storm events), as well as an order of magnitude increase in model decisions by simulating from different LOST_IN wave climate distributions each day. Daily LOST_IN could be useful for any application where the desired result is to identify a localized erosion hazard dependent on the chronology of individual storm events. However, direct comparisons of the shoreline model results from monthly
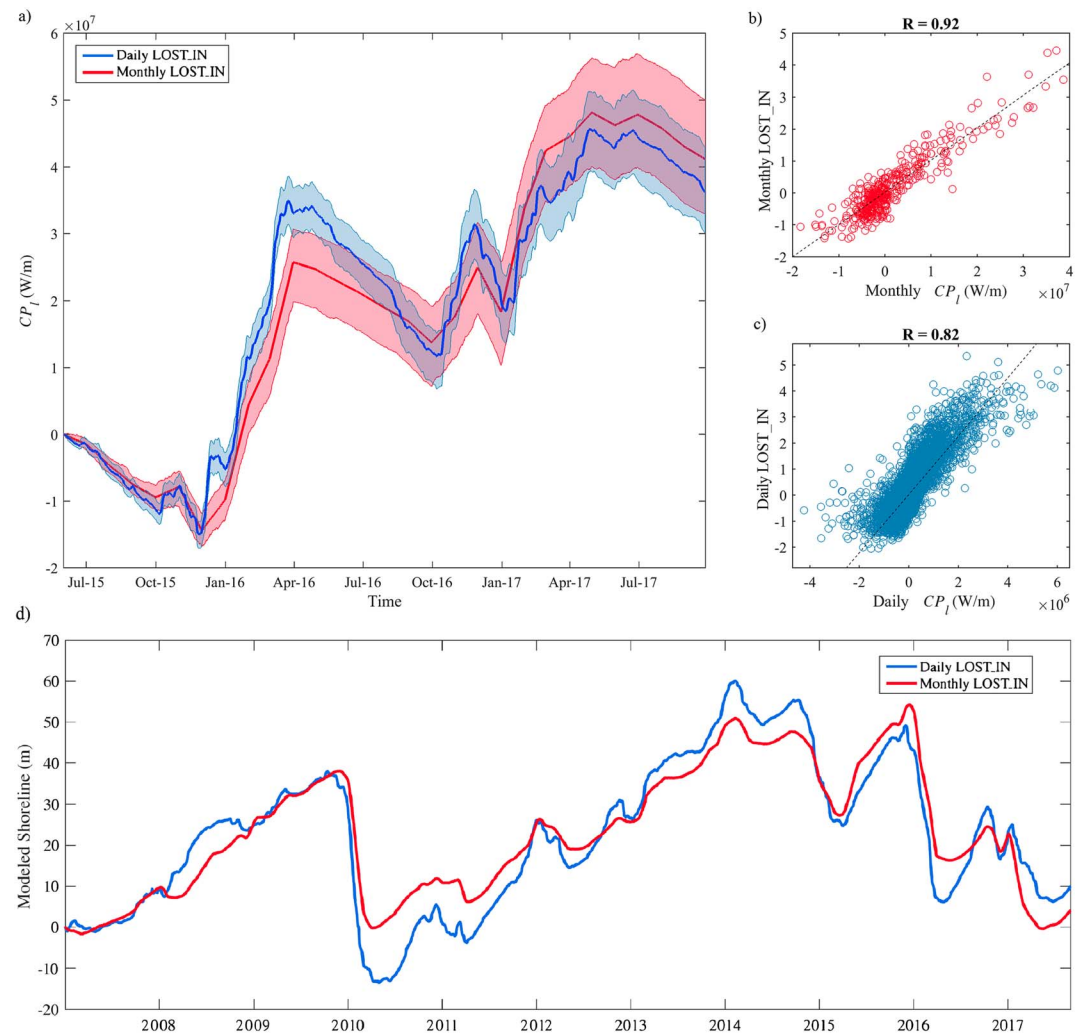
Figure 11. (a) One hundred simulations of ΣP_l from monthly LOST_IN (red) and daily LOST_IN (blue) where shaded areas are the maximum and minimum bounds of the simulation envelope and bold lines are the mean. (b) One-to-one correlation of monthly ΣP_l and monthly LOST_IN from 1979 to 2015 and (c) one-to-one correlation of daily ΣP_l and daily LOST_IN for the same time period. (d) Direct comparison of the same shoreline node in simulations with daily LOST_IN (red) and monthly LOST_IN (blue) waves during the most recent decade. LOST_IN = Longshore Sediment Transport Index.

LOST_IN versus daily LOST_IN suggest that the same interannual to decadal behavior is captured by the monthly LOST_IN (Figure 11d). The greater variance generated in ΣP_l from daily LOST_IN (Figure 11a) does not necessarily translate to significantly different shoreline simulations because the one-line model dynamically responds to the imposed wave climate, and because the long littoral cell requires large volumes of sand to be transported to produce a discernable rotation.

Although the results presented in Figure 11d are inherently a product of the one-line model assumptions and the large alongshore extent of the modeled littoral cell, the similarity of the shorelines presented for a model that resolves daily weather and one that lacks a chronology component suggest that rotational signals in the PNW may be less sensitive to individual weather events than the broader climate. The bounds associated with the 100 simulations of each model shown in Figure 11a quantify uncertainty inherent to the LOST_IN methodology, but also represent a range of possible shoreline change scenarios inherent to the climate of the last ~60 years. We have observed only one iteration of the coupled climate-meteorological system, where hourly weather is effectively noise super imposed on the large-scale signal. The framework presented in this paper creates the potential for examining multiple iterations of the climate, performed in a Monte Carlo sense. The computational efficiency associated with the statistical downscaling approach is order of

magnitude faster than performing multiple perturbations of a dynamic atmospheric model and coupling that with a wave model.

5.2. Meteorology of LOST_IN Bins

Several recent studies have correlated wave behavior and/or geomorphological response with climate indices (Barnard et al., 2015; Castelle et al., 2017; Poirier et al., 2017; T. Thomas et al., 2011). LOST_IN is unique in that it is an index optimally designed to emphasize a parameter driving morphological evolution (ΣP_l) while also retaining information concerning the climate that drives the evolution. Averaging the SLP fields within each LOST_IN bin provides a representative spatial pattern of the weather systems driving wave generation (Figure 12). Negative extremes of LOST_IN are associated with a strong high pressure system offshore of Oregon in the northeast Pacific Ocean (upper left corner of Figure 12), while positive extremes of LOST_IN exhibit strong Aleutian low pressures in the north Pacific Ocean and suppressed high pressures off of Southern California (lower right corner of Figure 12).

The location of the high pressure system in the northeast Pacific effectively steers storms tracking from west to east across the middle latitudes. A first-order approximation of storm tracks is the 1,014 mb geostrophic wind guide (e.g., Peterson et al., 1990), which shifts from making landfall ~55°N (Glacier Bay National Park, AK) in negative LOST_IN values to landfalls ~38°N (San Francisco, CA) during positive LOST_IN (dotted lines in Figure 12). The waves generated by a storm approaching southern Alaska and British Columbia propagate south to drive a southerly longshore component of wave power in Oregon, while those storms approaching central California propagate waves north to drive a northerly component of wave power. The most extreme LOST_IN bins identify storms that have been steered around the blocking high and low pressures such that they directly hit Oregon either steeply from the north (negative, upper left of Figure 12) or from the south (positive, lower right of Figure 12).

Climatologically, LOST_IN automatically identifies the likely magnitude and direction of a longshore component of wave power associated with potential storm tracks relative to the location of the study site. The quantitative link between the specific coastal process of interest and the spatial climate is unique relative to other statistical downscaling techniques. Other studies have developed techniques linking meteorological conditions with wave distributions (e.g., Antolinez et al., 2015; Rueda et al., 2017) by performing clustering analyses of the meteorology a priori to knowledge of wave conditions and forming coincident H_s, T_p, and θ distributions directly dependent on the atmospheric clusters. The present study differs from such previous work by clustering with respect to ΣP_l and is therefore identifying a specific nearshore process and the coincident meteorological conditions relevant to that process as opposed to vice versa. Rather than attempting to quantify all of the wave climate and atmospheric variability with the dynamic climate, the tailor-made climate index reduces dimensionality to minimize statistical uncertainty associated with the primary desired parameter. Wave climate variance was reduced from three dimensions to one dimension through the cumulative wave power parameter ΣP_l, while the multivariate regression further reduces the atmospheric variance needed to capture extremes in the meteorology forcing longshore wave power by choosing only EOFs relevant to this process. Such a framework could prove useful for identifying dominate meteorological patterns driving other coastal morphodynamic processes that are dependent on different forcing parameters (e.g., total wave energy driving evolution in a cross-shore equilibrium model; Yates et al., 2009).

5.3. Multidecadal Wave Climate Variability

The modeled shoreline evolution shown in Figure 8d suggests that a fundamental shift in the wave climate relevant to coastal change in north-central Oregon occurred in the late 1970s. The shift is easier to discern through extended ΣP_l time series of wave simulations produced from LOST_IN (Figure 13). A cumulative trend of predominantly southerly wave power persisted for several decades before a reversal and subsequent cumulative northerly wave power during the 1980s and 1990s. This trend reversal approximately coincides with a shift of the Pacific Decadal Oscillation (PDO) from its cool to warm phase (Figure 13a; Xue et al., 2014). Another regime shift of the PDO from warm back to cool is thought to have occurred in the late 1990s and persisted for two decades, which aside from the El Niño of 2009–2010 is composed of predominantly southerly directed ΣP_l. PDO is the dominant EOF mode of North Pacific sea surface temperatures, but an emerging consensus has identified that its behavior is not a single phenomenon but more a
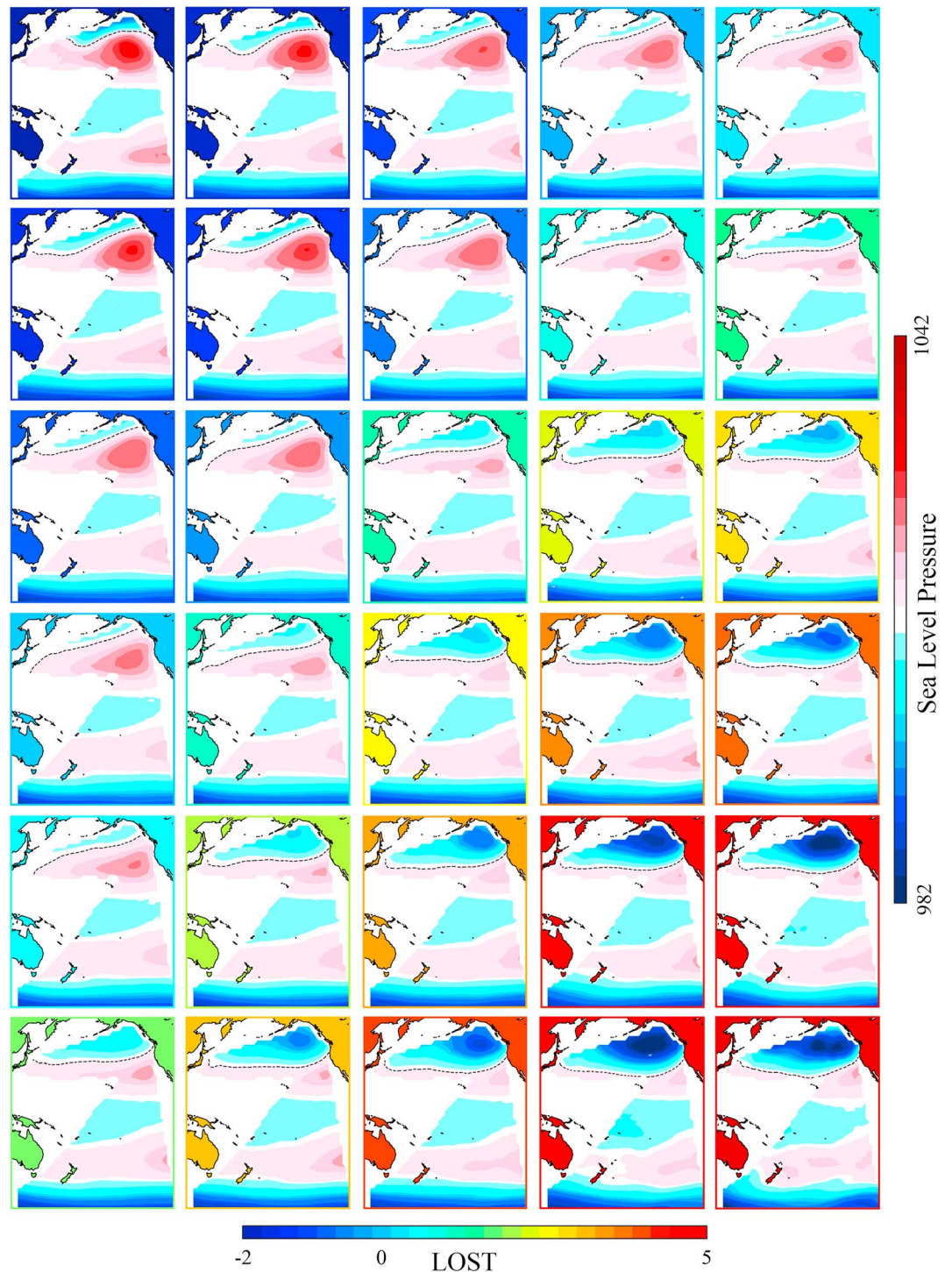
Figure 12. Average sea level pressure fields for LOST_IN separated into 30 bins. Color of the continents denotes the LOST_IN bin (same coordinated color as Figure 6) and the sea level pressures over the Pacific Ocean are presented as blues denoting lower than average pressures and reds denoting higher than average. Black dashed lines denote the 1,014 mb contour as a proxy for storm tracks moving from west to east across the North Pacific. LOST_IN = Longshore Sediment Transport Index.

function of multiple processes occurring in a much larger region, including remote and tropical forcing through atmospheric teleconnections (Newman et al., 2016). It is perhaps unsurprising that the extended ΣP_l record contains what appear to be coincident regime shifts with the most dominant mode of
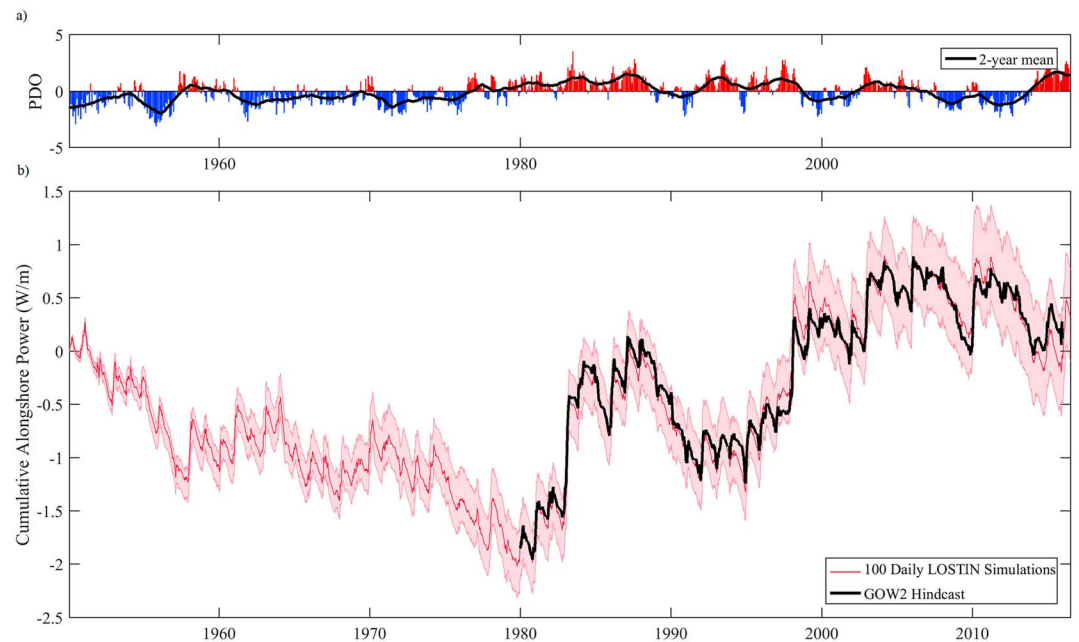
Figure 13. (a) Monthly PDO index values (obtain from University of Washington's JISAO climate data archive) with a 2-year rolling mean super imposed (black line) and (b) the mean (red line) and envelope of 100 simulations of hindcast cumulative longshore power ΣP_l using hourly wave derived from daily LOST_IN, as well as the GOW2 ΣP_l time series used to calibrate LOST_IN (black line). LOST_IN = Longshore Sediment Transport Index; GOW2 = Global Ocean Wave Reanalysis 2.0.

variability in the ocean adjacent to the PNW, but statistically significant correlations will require a longer observation window than the approximately one and a half PDO oscillations since the 1940s.

The approximately decadal scale oscillations observed in the shoreline results are superimposed on the PDO timescale in Figure 13. This insight regarding decadal and multidecadal behavior may change how coastal managers address future hazards in the region. Although quantitative data are limited, anecdotal evidence throughout the region provides examples of sand being passed back and forth between littoral cell extremities on comparable timescales to those revealed by LOST_IN. Pacific City homeowners (located in the northern end of a littoral cell ~45 km south of the Rockaway littoral cell; Figure 1) built riprap structures in the late 1970s due to persistent erosion of dunes and bluffs, which appears to coincide with three decades of southerly directed ΣP_l which would have moved sand from Pacific City to the south (Figure 13). By 1984, the riprap was buried beneath sand and the city needed excavators and bulldozers to dig houses out of the growing dunes (Allan et al., 2015). The time line of riprap burial coincides with the decade of northerly ΣP_l during the 1980s. The town of Neskowin at the opposing end of the littoral cell once had plenty of sand while Pacific City was hardening its shoreline, but has since installed multiple riprap structures in response to several decades of the beach in a persistent counterclockwise rotational state. While future coastal planning efforts along the north-central Oregon coast will need to consider sea level rise (Lipiec et al., 2018), coastal decision makers should also weigh the significant cost of building hard riprap structures within the context of interannual to multidecadal littoral cell rotations identified by this study.

5.4. Additional Applications

One advantage of statistical downscaling techniques such as LOST_IN is the ability to apply the technique to many locations with relatively little computational effort as compared to dynamic downscaling. LOST_IN can be applied to all headland-bound beaches in a region, or an ocean basin, to identify the dominant timescales and climatologies most affecting beach rotations or to investigate the spatial variability of such processes (e.g., Barnard et al., 2015). The ability of LOST_IN to fill in gaps in buoy records or extend the record of ΣP_l would be particularly useful in regions where wave information is scarce. The continuous time series produced by LOST_IN are essential for morphodynamic models dependent on chronological wave events such as the one presented in section 3, but the overall complexity of the methodology can be simplified by

transforming deep water wave conditions to the nearshore with linear shoaling and refraction rather than the dynamic lookup table used in this study.

Equation (4) could also be applied to forecasted SLP fields from general circulation models (GCMs), turning LOST_IN_Oregon into a predictive tool. Current changes to the global climate are projected to alter large-scale atmospheric circulations; shift weather and wind patterns, storm tracks, and storm intensities; and consequently alter future wave climates throughout the world (Erikson et al., 2015; Hemer et al., 2013). However, the quality of the $\sum P_l$ prediction is inherently tied to the ability of GCMs to reproduce relevant timescales of variability, and the North Pacific is a region where GCMs have difficulty recreating low frequency modulations of the climate (Branstator et al., 2012; Comeau et al., 2017). Ad hoc hypothetical climates could still be considered using the LOST_IN framework until GCMs replicate the necessary timescales of complexity. The methodology identifies the relevant EOFs and associated PC chronologies during the last 60 years of El Niños, providing the necessary information to simulate atmospheric variability and investigate how predicted changes in El Niño frequency may affect pocket beach rotation behavior in the 21st century.

6. Conclusions

This paper presents LOST_IN_Oregon, a framework developed to statistically downscale climate variability through an index optimized to capture longshore wave power as the environmental force morphologically controlling shoreline evolution. The framework creates a predictive equation for longshore wave power through a multivariate regression between historical $\sum P_l$ and EOFs of SLP fields in regions generating wave energy that propagates to north-central Oregon. The predictive equation can be applied to any time period with SLP data (or SLP forecasts), extending records of $\sum P_l$ by filling in gaps in wave observation records or investigating possible shoreline change scenarios associated with alternate iterations of the climate-weather system.

Shoreline model results utilizing wave simulations derived from LOST_IN reveal timescales of headland-bound littoral cell rotation in the PNW not previously identified from the available observations. As anticipated, El Niños are a relevant climate phenomenon contributing to rotation, but such events are superimposed on interannual and multidecadal climate oscillations that result in persistent shoreline rotations. A relationship between the spatial influence of headlands and the shoreline's sensitivity to interannual wave climate variability was also discernible in the simple one-line model results. Close to the headlands, interannual to decadal oscillations contribute to rotational signals, while the impact of El Niño winters on alongshore processes is limited to localities in the immediately vicinity of headlands, inlets, or jetties. The strong dependency of shoreline orientation on wave climate variability suggests that projected changes in the 21st century climate (i.e., increased frequency of El Niños, Cai et al., 2014, and northerly shifts of storm tracks, Erikson et al., 2015) may have a profound effect on the coastal evolution of the PNW.

References

Allan, J. C., & Hart, R. (2008). Oregon beach and shoreline mapping and analysis program: 2007-2008 beach monitoring report: Oregon Department of Geology and Mineral Industries Open-File Report 0-08-15.

Allan, J. C., & Komar, P. D. (2006). Climate controls on US West Coast erosion processes. *Journal of Coastal Research*, *223*(3), 511–529. https://doi.org/10.2112/03-0108.1

Allan, J. C., Komar, P. D., & Priest, G. R. (2003). Shoreline variability on the high-energy Oregon coast and its usefulness in Erosion-hazard assessments. *Journal of Coastal Research*, *38*, 83–105. Retrieved from www.jstor.org/stable/25736601

Allan, J. C., Ruggiero, P., Garcia-Medina, G., O'Brien, F., Stimely, L., & Roberts, J. (2015). Coastal flood hazard study, Tillamook County Oregon. Special Paper 47, Oregon Department of Geology and Mineral Industries.

Antolínez, J. A., Murray, A. B., Méndez, F. J., Moore, L. J., Farley, G., & Wood, J. (2018). Downscaling changing coastlines in a changing climate: The hybrid approach. *Journal of Geophysical Research: Earth Surface*, *123*, 229–251. https://doi.org/10.1002/2017JF004367

Antolinez, J. A. A., Mendez, F. J., Camus, P., Vitousek, S., Gonzalez, E. M., Ruggiero, P., & Barnard, P. L. (2015). A multiscale climate emulator for long-term morphodynamics (MUSCLE-morpho). *Journal of Geophysical Research: Oceans*, *120*, 1152–1172. https://doi.org/10.1002/2014JC010299

Archetti, R., & Romagnoli, C. (2011). Analysis of the effects of different storm events on shoreline dynamics of an artificially embayed beach. *Earth Surface Processes and Landforms*, *36*(11), 1449–1463. https://doi.org/10.1002/esp.2162

Barnard, P. L., Hoover, D., Hubbard, D. M., Snyder, A., Ludka, B. C., Allan, J., & Serafin, K. A. (2017). Extreme oceanographic forcing and coastal response due to the 2015-2016 El Niño. *Nature Communications*, *8*, 1–8. https://doi.org/10.1038/ncomms14365

Barnard, P. L., Short, A. D., Harley, M. D., Splinter, K. D., Vitousek, S., Turner, I. L., et al. (2015). Coastal vulnerability across the Pacific dominated by El Nino/Southern Oscillation. *Nature Geoscience*, *8*(10), 801–807. https://doi.org/10.1038/NGEO2539

Bayram, A., Larson, M., & Hanson, H. (2007). A new formula for the total longshore sediment transport rate. *Coastal Engineering*, *54*(9), 700–710. https://doi.org/10.1016/j.coastaleng.2007.04.001

Blossier, B., Bryan, K. R., & Winter, C. (2017). Shore and bar cross-shore migration, rotation, and breathing processes at an embayed beach. *Journal of Geophysical Research: Earth Surface*, *122*, 1745–1770. https://doi.org/10.1002/2017JF004227

Booij, N., Ris, R. C., & Holthuijsen, L. H. (1999). A third-generation wave model for coastal regions: 1. Model description and validation. *Journal of Geophysical Research*, *104*(C4), 7649–7666. https://doi.org/10.1029/98JC02622

Branstator, G., Teng, H., Meehl, G. A., Kimoto, M., Knight, J. R., Latif, M., & Rosati, A. (2012). Systematic estimates of initial-value decadal predictability for six AOGCMs. *Journal of Climate*, *25*(6), 1827–1846. https://doi.org/10.1175/JCLI-D-11-00227.1

Bryan, K. R., Foster, R., & MacDonald, I. (2013). Beach rotation at two adjacent headland-enclosed beaches. *Journal of Coastal Research: Special Issue 65 - International Coastal Symposium*, *2*, 2095–2100. https://doi.org/10.2112/SI65-354

Cai, W., Borlace, S., Lengaigne, M., van Rensch, P., Collins, M., Vecchi, G., et al. (2014). Increasing frequency of extreme El Niño events due to greenhouse warming. *Nature Climate Change*, *4*(2), 111–116. https://doi.org/10.1038/nclimate2100

Camus, P., Méndez, F. J., Losada, I. J., Menéndez, M., Espejo, A., Pérez, J., et al. (2014). A method for finding the optimal predictor indices for local wave climate conditions. *Ocean Dynamics*, *64*(7), 1025–1038. https://doi.org/10.1007/s10236-014-0737-2

Camus, P., Menéndez, M., Méndez, F. J., Izaguirre, C., Espejo, A., Cánovas, V., et al. (2014). A weather-type statistical downscaling framework for ocean wave climate. *Journal of Geophysical Research: Oceans*, *119*, 7389–7405. https://doi.org/10.1002/2014JC010141

Casas-Prat, M., Wang, X. L., & Sierra, J. P. (2014). A physical-based statistical method for modeling ocean wave heights. *Ocean Modelling*, *73*, 59–75. https://doi.org/10.1016/j.ocemod.2013.10.008

Castelle, B., Dodet, G., Masselink, G., & Scott, T. (2017). A new climate index controlling winter wave activity along the Atlantic coast of Europe: The West Europe Pressure Anomaly. *Geophysical Research Letters*, *44*, 1384–1392. https://doi.org/10.1002/2016GL072379

Cohn, N., Ruggiero, P., de Vries, S., & Garcia-Medina, G. (2017). Beach growth driven by intertidal sandbar welding. In T. Aagaard, R. Deigaard, & D. Fuhrman (Eds.), *Proceedings of coastal dynamics 2017* (pp. 1059–1069). Denmark: Helsingor.

Comeau, D., Zhao, Z., Giannakis, D., & Majda, A. J. (2017). Data-driven prediction strategies for low-frequency patterns of North Pacific climate variability. *Climate Dynamics*, *48*(5–6), 1855–1872. https://doi.org/10.1007/s00382-016-3177-5

Daly, C. J., Bryan, K. R., & Winter, C. (2014). Wave energy distribution and morphological development in and around the shadow zone of an embayed beach. *Coastal Engineering*, *93*, 40–54. https://doi.org/10.1016/j.coastaleng.2014.08.003

Davidson, M., Van Koningsveld, M., de Kruif, A., Rawson, J., Holman, R., Lamberti, A., et al. (2007). The CoastView project: Developing video-derived coastal state indicators in support of coastal zone management. *Coastal Engineering*, *54*(6–7), 463–475. https://doi.org/10.1016/j.coastaleng.2007.01.007

Davidson, M. A., Turner, I. L., Splinter, K. D., & Harley, M. D. (2017). Annual prediction of shoreline erosion and subsequent recovery. *Coastal Engineering*, *130*, 14–25. https://doi.org/10.1016/j.coastaleng.2017.09.008

Elko, N., Feddersen, F., Foster, D., Hapke, C., Mcninch, J., Mulligan, R., et al. (2014, December). *The future of nearshore processes research*. Abstract OS22A-08 presented at 2014 Fall Meeting, AGU, San Francisco, CA.

Elshinnawy, A. I., Medina, R., & Gonzalez, M. (2017). On the relation between the direction of the wave energy flux and the orientation of equilibrium beaches. *Coastal Engineering*, *127*, 20–36. https://doi.org/10.1016/j.coastaleng.2017.06.009

Erikson, L. H., Hegermiller, C. A., Barnard, P. L., Ruggiero, P., & van Ormondt, M. (2015). Projected wave conditions in the eastern North Pacific under the influence of two CMIP5 climate scenarios. *Ocean Modelling*, *96*, 171–185. https://doi.org/10.1016/j.ocemod.2015.07.004

Fenster, M., & Dolan, R. (1994). Large-scale reversals in shoreline trends along the US mid-Atlantic coast. *Geology*, *22*(6), 543–546. https://doi.org/10.1130/0091-7613(1994)022<0543:LSRIST>2.3.CO;2

Hanson, J. L., Tracy, B. A., Tolman, H. L., & Scott, R. D. (2009). Pacific hindcast performance of three numerical wave models. *Journal of Atmospheric and Oceanic Technology*, *26*(8), 1614–1633. https://doi.org/10.1175/2009JTECHO650.1

Harley, M. D., Andriolo, U., Armaroli, C., & Ciavola, P. (2014). Shoreline rotation and response to nourishment of a gravel embayed beach using a low-cost video monitoring technique: San Michele-Sassi Neri, Central Italy. *Journal of Coastal Conservation*, *18*(5), 551–565. https://doi.org/10.1007/s11852-013-0292-x

Harley, M. D., Turner, I. L., & Short, A. D. (2015). New insights into embayed beach rotation: The importance of wave exposure and cross-shore processes. *Journal of Geophysical Research: Earth Surface*, *120*, 1470–1484. https://doi.org/10.1002/2014JF003390

Harley, M. D., Turner, I. L., Short, A. D., & Ranasinghe, R. (2011). A reevaluation of coastal embayment rotation: The dominance of cross-shore versus alongshore sediment transport processes, Collaroy-Narrabeen Beach, southeast Australia. *Journal of Geophysical Research*, *116*, F04033. https://doi.org/10.1029/2011JF001989

Hegermiller, C. A., Antolinez, J. A. A., Rueda, A., Camus, P., Perez, J., Erikson, L., et al. (2017). A multimodal wave Spectrum – Based approach for statistical downscaling of local wave climate. *American Meteorological Society*, *47*(February), 375–386. https://doi.org/10.1175/JPO-D-16-0191.1

Hemer, M. a., Fan, Y., Mori, N., Semedo, A., & Wang, X. L. (2013). Projected changes in wave climate from a multi-model ensemble. *Nature Climate Change*, *3*(5), 471–476. https://doi.org/10.1038/nclimate1791

Hurst, M. D., Barkwith, A., Ellis, M. A., Thomas, C. W., & Murray, A. B. (2015). Exploring the sensitivities of crenulate bay shorelines to wave climates using a new vector-based one-line model. *Journal of Geophysical Research: Earth Surface*, *120*, 2586–2608. https://doi.org/10.1002/2015JF003704

Johnson, J. M., Moore, L. J., Ells, K., Murray, A. B., Adams, P. N., Mackenzie, R. A., & Jaeger, J. M. (2015). Recent shifts in coastline change and shoreline stabilization linked to storm climate change. *Earth Surface Processes and Landforms*, *40*(5), 569–585. https://doi.org/10.1002/esp.3650

Kalnay, E., Kanamitsu, M., Kistler, R., Collins, W., Deaven, D., Gandin, L., et al. (1996). The NCEP/NCAR 40-year reanalysis project. *Bulletin of the American Meteorological Society*, *77*(3), 437–471. https://doi.org/10.1175/1520-0477(1996)077<0437:TNYRP>2.0.CO;2

Kaminsky, G. M., Ruggiero, P., & Gelfenbaum, G. (1998). Monitoring coastal change in southwest Washington and northwest Oregon during the 1982-83 El Niño. *Shore and Beach*, *66*(3), 42–51.

Kamphuis, B. J. W. (1992). Alongshore sediment transport rate. *Journal of Waterway, Port, Coastal, and Ocean Engineering*, *117*(6), 624–640. https://doi.org/10.1061/(ASCE)0733-950X(1991)117:6(624)

Kistler, R., Kalnay, E., Collins, W., Saha, S., White, G., Woollen, J., et al. (2001). The NCEP-NCAR 50-year reanalysis: Monthly means CD-ROM and documentation. *Bulletin of the American Meteorological Society*, *82*(2), 247–267. https://doi.org/10.1175/1520-0477(2001)082<0247:TNNYRM>2.3.CO;2

Komar, P. D. (1986). The 1982-83 El Niño and erosion on the coast or Oregon. *Shore and Beach*, *54*(2), 3–12.

Komar, P. D. (1998a). *Beach processes and sedimentation* (2nd ed., 544 pp.). Upper Saddle River, NJ: Prentice Hall.

Komar, P. D. (1998b). The 1997-98 El Niño and Erosion on the Oregon coast. *Shore and Beach*, *66*(3), 33–41. https://doi.org/10.1017/CBO9781107415324.004

Komar, P. D., & Allan, J. C. (2008). Increasing hurricane-generated wave heights along the US east coast and their climate controls. *Journal of Coastal Research*, *242*(2), 479–488. https://doi.org/10.2112/07-0894.1

Komar, P. D., & Inman, D. L. (1970). Longshore sand transport on beaches. *Journal of Geophysical Research*, *75*(30), 5914–5927. https://doi.org/10.1029/JC075i030p05914

Lipiec, E., Ruggiero, P., Mills, A., Serafin, K. A., Bolte, J., Corcoran, P., et al. (2018). Mapping out climate change: Assessing how coastal communities adapt using alternative future scenarios. *Journal of Coastal Research*. https://doi.org/10.2112/JCOASTRES-D-17-00115

Masselink, G., & Pattiaratchi, C. B. (2001). Seasonal changes in beach morphology along the sheltered coastline of Perth, Western Australia. *Marine Geology*, *172*(3–4), 243–263. https://doi.org/10.1016/S0025-3227(00)00128-6

Mil-Homens, J., Ranasinghe, R., van Thiel de Vries, J. S. M., & Stive, M. J. F. (2013). Re-evaluation and improvement of three commonly used bulk longshore sediment transport formulas. *Coastal Engineering*, *75*, 29–39. https://doi.org/10.1016/j.coastaleng.2013.01.004

Newman, M., Alexander, M. A., Ault, T. R., Cobb, K. M., Deser, C., Di Lorenzo, E., & Smith, C. A. (2016). The Pacific decadal oscillation, revisited. *Journal of Climate*, *29*(12), 4399–4427. https://doi.org/10.1175/JCLI-D-15-0508.1

Pelnard-Considere, R. (1956). Essai de theorie de l'evolution des dorms de ravage en plages de sable det de galets. *Journees de l'Hydraulique, Les Energies de La Mer*, *4*, 289–298.

Perez, J., Mendez, F. J., Menendez, M., & Losada, I. J. (2014). ESTELA: A method for evaluating the source and travel time of the wave energy reaching a local area. *Ocean Dynamics*, *64*(8), 1181–1191. https://doi.org/10.1007/s10236-014-0740-7

Perez, J., Menendez, M., Camus, P., Mendez, F. J., & Losada, I. J. (2015). Statistical multi-model climate projections of surface ocean waves in Europe. *Ocean Modelling*, *96*, 161–170. https://doi.org/10.1016/j.ocemod.2015.06.001

Perez, J., Menendez, M., & Losada, I. J. (2017). GOW2: A global wave hindcast for coastal applications. *Coastal Engineering*, *124*(April), 1–11. https://doi.org/10.1016/j.coastaleng.2017.03.005

Peterson, C. D., Jackson, P. L., O'Neil, D. J., Rosenfeld, C. L., & Kimerling, A. J. (1990). Littoral cell response to interannual climatic forcing 1983-1987 on the Central Oregon coast, USA. *Journal of Coastal Research*, *6*(1), 87–110.

Pilkey, O. H., & Cooper, J. A. G. (2002). Longshore Transport Volumes: A Critical View. *Journal of Coastal Research: Special Issue 36 - International Coastal Symposium (ICS 2002)*, 572–580. https://doi.org/10.2112/1551-5036-36.sp1.572

Poirier, C., Tessier, B., Chaumillon, É., Bertin, X., Fruergaard, M., Mouazé, D., et al. (2017). Decadal changes in North Atlantic atmospheric circulation patterns recorded by sand spits since 1800 CE. *Geomorphology*, *281*, 1–12. https://doi.org/10.1016/j.geomorph.2016.12.028

Ranasinghe, R. (2016). Assessing climate change impacts on open sandy coasts: A review. *Earth Science Reviews*, *160*, 320–332. https://doi.org/10.1016/j.earscirev.2016.07.011

Ranasinghe, R., McLoughlin, R., Short, A., & Symonds, G. (2004). The Southern Oscillation Index, wave climate, and beach rotation. *Marine Geology*, *204*(3–4), 273–287. https://doi.org/10.1016/S0025-3227(04)00002-7

Ratliff, K. M., & Murray, A. B. (2014). Modes and emergent time scales of embayed beach dynamics. *Geophysical Research Letters*, *41*, 7270–7275. https://doi.org/10.1002/2014GL061680

Revell, D. L., Komar, P. D., & Sallenger, A. H. Jr. (2002). An application of LIDAR to analyses of El Niño erosion in the Netarts littoral cell, Oregon. *Journal of Coastal Research*, *18*(4), 792–801.

Roelvink, D., & Reniers, A. (2012). A guide to modeling coastal morphology. In *Advances in coastal and ocean engineering (Advances I), Morphological Processes* (pp. 111–143). Singapore: World Scientific Publishing Company. https://doi.org/10.1142/9789814304269_0005

Roelvink, J. A. (2006). Coastal morphodynamic evolution techniques. *Coastal Engineering*, *53*(2–3), 277–287. https://doi.org/10.1016/j.coastaleng.2005.10.015

Rueda, A., Hegermiller, C. A., Antolinez, J. A. A., Camus, P., Vitousek, S., Ruggiero, P., et al. (2017). Multiscale climate emulator of multimodal wave spectra: MUSCLE-spectra. *Journal of Geophysical Research: Oceans*, *122*, 1400–1415. https://doi.org/10.1002/2016JC011957

Ruggiero, P., Buijsman, M., Kaminsky, G. M., & Gelfenbaum, G. (2010). Modeling the effects of wave climate and sediment supply variability on large-scale shoreline change. *Marine Geology*, *273*(1–4), 127–140. https://doi.org/10.1016/j.margeo.2010.02.008

Ruggiero, P., Kaminsky, G. M., & Plant, N. G. (1998). Coastal morphologic variability of high energy dissipative beaches. 26th International Conference on Coastal Engineering, Copenhagen, DK, (31), 3238–3251.

Ruggiero, P., Komar, P. D., & Allan, J. C. (2010). Increasing wave heights and extreme value projections: The wave climate of the U.S. Pacific Northwest. *Coastal Engineering*, *57*(5), 539–552. https://doi.org/10.1016/j.coastaleng.2009.12.005

Ruggiero, P., Kratzmann, M. G., Himmelstoss, E. A., Reid, D., Allan, J., & Kaminsky, G. (2013). National assessment of shoreline change: Historical shoreline change along the Pacific Northwest coast. doi: https://doi.org/10.3133/ofr20121007

Ruiz de Alegria-Arzaburu, A., & Masselink, G. (2010). Storm response and beach rotation on a gravel beach, Slapton Sands, U.K. *Marine Geology*, *278*(1–4), 77–99. https://doi.org/10.1016/j.margeo.2010.09.004

Serafin, K. A., & Ruggiero, P. (2014). Simulating extreme total water levels using time-dependent, extreme value approach. *Journal of Geophysical Research: Oceans*, *119*, 6305–6329. https://doi.org/10.1002/2014JC010093

Short, A. D., & Masselink, G. (1999). Embayed and structurally controlled beaches. In A. D. Short (Ed.), *Handbook of beach and shoreface morphodynamics* (pp. 230–249). Chichester, UK: John Wiley.

Slott, J. M., Murray, A. B., Ashton, A. D., & Crowley, T. J. (2006). Coastline responses to changing storm patterns. *Geophysical Research Letters*, *33*(18), L18404. https://doi.org/10.1029/2006GL027445

Smith, E. R., Wang, P., Ebersole, B. A., & Zhang, J. (2009). Dependence of total longshore sediment transport rates on incident wave parameters and breaker type. *Journal of Coastal Research*, *25*(3), 675–683. http://www.jstor.org/stable/27698361

Stive, M. J. F., Aarninkhof, S. G. J., Hamm, L., Hanson, H., Larson, M., Wijnberg, K. M., et al. (2002). Variability of shore and shoreline evolution. *Coastal Engineering*, *47*(2), 211–235. https://doi.org/10.1016/S0378-3839(02)00126-6

Thomas, C. W., Murray, A. B., Ashton, A. D., Hurst, M. D., Barkwith, A. K. A. P., & Ellis, M. A. (2016). Complex coastlines responding to climate change: Do shoreline shapes reflect present forcing or "remember" the distant past? *Earth Surface Dynamics*, *4*(4), 871–884. https://doi.org/10.5194/esurf-4-871-2016

Thomas, T., Phillips, M. R., Williams, A. T., & Jenkins, R. E. (2011). Short-term beach rotation, wave climate and the North Atlantic Oscillation (NAO). *Progress in Physical Geography*, *35*(3), 333–352. https://doi.org/10.1177/0309133310397415

Tolman, H. L. (2002). Validation of WAVEWATCH III version 1.15 for a global domain. NOAA/NWS/NCEP/OMB, 213, 33.

Turki, I., Medina, R., Coco, G., & Gonzalez, M. (2013). An equilibrium model to predict shoreline rotation of pocket beaches. *Marine Geology*, *346*, 220–232. https://doi.org/10.1016/j.margeo.2013.08.002

Vitousek, S., Barnard, P. L., & Limber, P. (2017). Can beaches survive climate change? *Journal of Geophysical Research: Earth Surface*, *122*, 1060–1067. https://doi.org/10.1002/2017JF004308

Vitousek, S., Barnard, P. L., Limber, P., Erikson, L. H., & Cole, B. (2017). A model integrating longshore and cross-shore processes for predicting long-term shoreline response to climate change. *Journal of Geophysical Research: Earth Surface*, *122*, 782–806. https://doi.org/10.1002/2016JF004065

Wang, X. L., Feng, Y., & Swail, V. R. (2012). North Atlantic wave height trends as reconstructed from the 20th century reanalysis. *Geophysical Research Letters*, *39*, L18705. https://doi.org/10.1029/2012GL053381

Wang, X. L., Zwiers, F. W., & Swail, V. R. (2004). North Atlantic Ocean wave climate change scenarios for the twenty-first century. *Journal of Climate*, *17*(12), 2368–2383. https://doi.org/10.1175/1520-0442(2004)017<2368:NAOWCC>2.0.CO;2

WAVEWATCH III Development Group (WW3DG) (2016). *User manual and system documentation of WAVEWATCH III version 5.16. Tech. Note 329* (p. 326). College Park, MD: NOAA/NWS/NCEP/MMAB.

Xue, Y., Hu, Z., Banzon, V., Smith, T. M., & Rayner, N. A. (2014). Global Sea Surface Temperatures in State of the Climate in 2013.

Yates, M. L., Guza, R. T., & O'Reilly, W. C. (2009). Equilibrium shoreline response: Observations and modeling. *Journal of Geophysical Research*, *114*, C09014. https://doi.org/10.1029/2009JC005359